1978

Gamma ray radiation studies of undoped GaAs

William P. Winfree
College of William & Mary - Arts & Sciences

GAMMA RAY RADIATION STUDIES OF UNDOPED GaAs

GAMMA RAY RADIATION STUDIES OF UNDOPED GaAs

A Dissertation

Presented to

The Faculty of the Department of Physics

The College of William and Mary in Virginia

In Partial Fulfillment

Of the Requirements for the Degree of

Doctor of Philosophy

---

by

William P. Winfree

1978

APPROVAL SHEET

This dissertation is submitted in partial fulfillment of

the requirements for the degree of

Doctor of Philosophy

William P. Winfree
Author

Approved, September 1978

J. F. Soest
J. F. Soest, Chairman

A. Sher
A. Sher

H E Schone
H. E. Schone

W. J. Kossler
W. J. Kossler

R. A. Breckenridge
R. A. Breckenridge
NASA-Langley Research Center

TABLE OF CONTENTS

ACKNOWLEDGMENTS

I wish to express my gratitude to the following persons: M. K. Cueman and R. K. Hester for instruction in use of the basic spectrometer; K. A. Dumas for assistance in taking data; J. F. Soest for experimental direction and serving as my thesis advisor; A. Sher for his interest in the experiment and guidance in the theoretical portions. H. E. Schone, W. J. Kossler and R. A. Breckenridge for helpful suggestions and serving on my examination committee. B. Burkett for typing the first draft, and moral support; R. Bryant for the final typing of the manuscript.

LIST OF TABLES

LIST OF FIGURES

ABSTRACT

High purity GaAs crystals were irradiated at room temperature with gamma rays. Pulsed NMR was then used to measure the effect of any stable defects introduced into the samples. No increases in the number of stable defects were found as a consequence of irradiating these samples. The carrier concentrations of the samples also did not change appreciably. This was determined by examining the temperature dependence of the NMR decay shape and by an independent measurement of the carrier concentration. We suggest the following model to explain the absence of the new stable defects. The Frenkel pairs created by the irradiation are mobile. In our high purity sample these mobile defects anneal because there are few impurities with which they can interact to form complexes. Complex formation is the mechanism that stabilizes the radiation introduced defects in prior experiments done on less pure samples.

Additional evidence for a high mobility of the defects in this pure sample can be deduced from other measurements which indicate the self diffusion constant is greater than the value quoted in the literature. GaAs samples were held at elevated temperatures, from 550°C to 700°C, in an evacuated chamber for twenty four hours and the quench cooled to room temperature. The spatial distribution of the resulting defects is a measure of the self diffusion coefficient of the material. The degree of homogeneity of these samples was measured using pulsed NMR on slices of the samples. The degree of homogeneity was then used to estimate a lower limit of the pure GaAs self diffusion constant for the temperatures at which it was thermally damaged. The lower limit we found is much greater than the value for the self diffusion constant quoted in the literature.

GAMMA RAY RADIATION STUDIES

OF UNDOPED GaAs

I. INTRODUCTION

Because GaAs is the best controlled among the III-V compound semiconductors, and it has properties that are exceedingly useful for a broad range of important devices, it has been thoroughly investigated. In particular, extensive studies have been conducted on the effects of radiation damage on its transport properties[1]. Previous experiments conducted at our lab have concentrated on damage to high purity GaAs by gamma rays from a Co^{60} source. The focus on gamma ray induced damage results from their long penetration depth, that produces uniform damage in the relatively large crystals required for nuclear magnetic resonance experiments.

Gamma ray damage to solids is not caused by a direct interaction between the photon and the nuclei in the lattice. The gamma rays scatter electrons elastically (Compton scattering)[2], which have a short mean free path, then interact with the nuclei, causing them to be displaced in the lattice. Since the damage is actually caused by the scattered electrons rather than the gamma rays, the type of damage introduced by gamma rays similar to that found in electron irradiation experiments. The one exception occurs for relatively large crystals where the damage from gamma irradiation is uniformly distributed in the crystal, while for direct electron irradiation the damage is concentrated near the surface.

The gamma rays from the Co^{60} source produce electrons with approximately 1 MeV of energy or less. For these relatively low energy electrons, displacement of more than one atom per electron is rare[2]. The damage then consists mostly of singly displaced atoms resulting in vacancy-interstitial pairs (Frenkel defects). For low energy electrons, a high degree of correlation between the two elements of a Frenkel pair is expected.

Experimental attempts have been made to determine the exact nature of the defects created by electrons and gamma irradiations. Earlier work focused on the change induced in macroscopic properties of the material, such as the carrier concentration and the mobility. These features were studied as a function of total dose, dose rate and subsequent annealling characteristics[3]. Recently, Lang and Kimerling[4] developed a new technique to measure the ionization energy of traps introduced by irradiation. Thus, they have a way to characterize the centers that are created. Jeong et. al.[5] identified one of the complexes formed after annealing the irradiation damage. However, no experiment or collection of experiments provide enough information to identify all the stable defects formed by irradiation.

Our experiment was designed to add to the knowledge about these defects and to facilitate their identification. The experiment measures the number of new stable charged defects created by the irradiation. The method depends on a theory derived independently by Fedders[6] and Cueman et. al.[7] to deduce the charge defect concentrations from the measurement. The theory predicts the functional

dependence of the shape of the nuclear magnetic free induction decay on the charge defect density of the sample.

The NMR spectrometer is described in Chapter II. The line shape theory is modified in Chapter III to include the effect of screening of internal electric fields by the charge carriers present. The experimental technique used to measure the defect density of the sample is discussed in detail in Chapter IV. The actual experiments done on the GaAs samples and their results are presented in Chapter V. These results are discussed and compared to those of others in Chapter VI.

II. EQUIPMENT

The basic spectrometer was reported by Hester[8] and Cueman[9] in their respective dissertations. The following modifications have been made.

A. Power Amplifier

The NMR Specialities power amplifier was replaced by a solid state ENI (Electronic Navigation Industries) A-300 broad band amplifier. The A-300 is a linear 300-watt CW amplifier, with a bandwidth of 0.3 to 35 MHz and 55 db of gain. Unlike the NMR Specialities amplifier, it is not gated. Therefore, the following changes have been made in the rest of the system to compensate for this fact.

An additional gate is required on the RF input coming to the amplifier from the pulse programmer. Without this gate, the output of the power amplifer is 0.5 volts peak to peak, when it is supposed to be zero. With the additional gate the output level of the amplifier is 0.02 volts peak to peak. This latter output is a result of noise generated within the power amplifier, and cannot be reduced by further gating of the input.

One set of diodes is not sufficient to decouple this output noise from the receiver of the spectrometer. An additional set of diodes as well as two PIN diodes were placed in series with the already exisitng set of diodes as shown in Fig. 1. A quarter wavelength cable for the

Figure 1. Changes to the spectrometer to decouple power amplifier output from the receiver

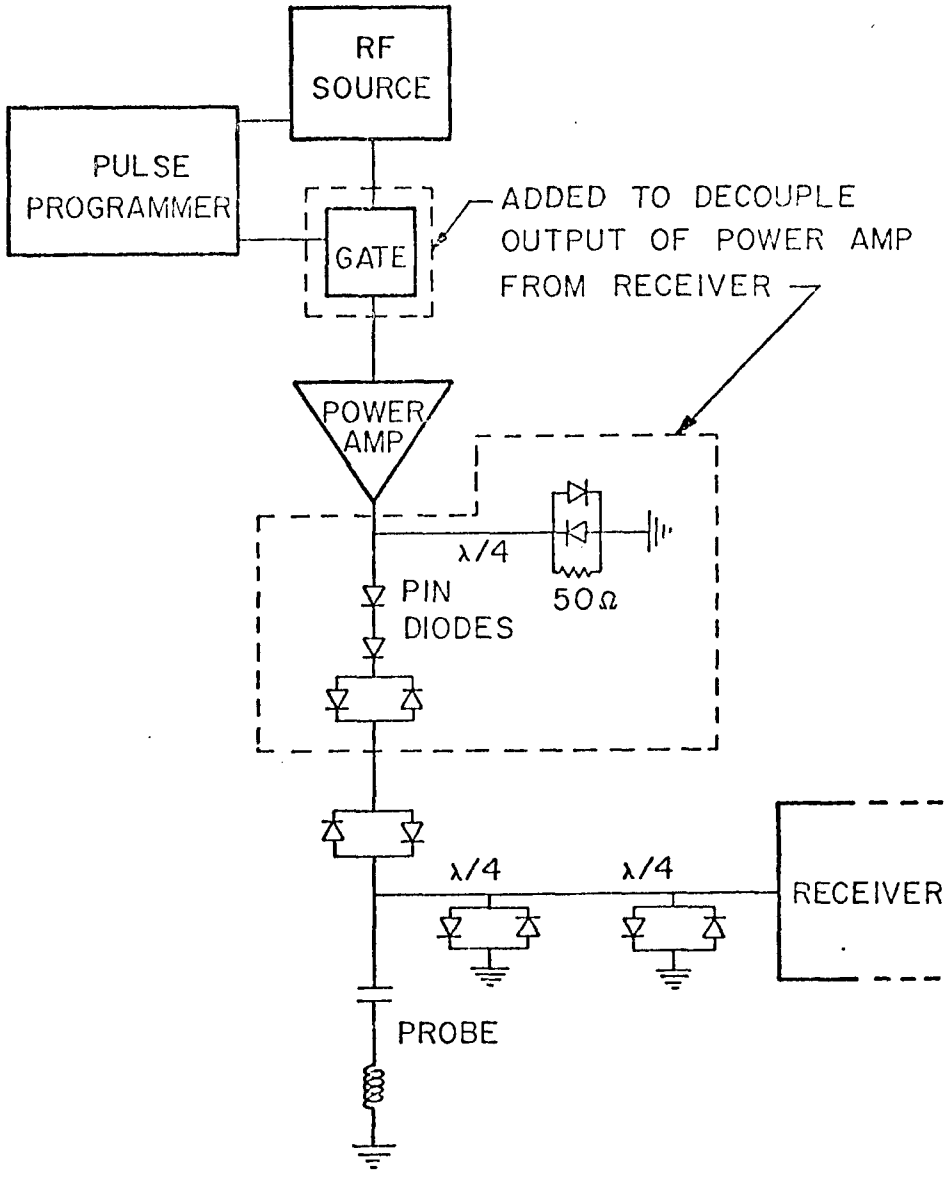
RF SOURCE
PULSE PROGRAMMER
GATE
ADDED TO DECOUPLE OUTPUT OF POWER AMP FROM RECEIVER
POWER AMP
λ/4
PIN DIODES
50Ω
λ/4
λ/4
RECEIVER
PROBE

resonance frequency is placed in parallel with the probe at the output of the power amplifier also as shown in Fig. 1. A set of diodes to ground in parallel with a 50Ω resistor is placed at the end of this cable. At the output of the amplifier this cable looks open when the pulse is on. When the pulse is off, it presents the output with a 50Ω power dissipating load.[10]

B. Liquid Nitrogen Probe

A liquid nitrogen dewar was purchased from Pope Scientific, Inc. A new probe that would fit in the dewar was designed. A diagram of this probe is shown in Fig. 2.

Experience with high voltage ceramic disk capacitors shows that their capacitance changes by 2 to 3 orders of magnitude between room temperature and liquid nitrogen temperature. Tuning a circuit with them at liquid nitrogen temperature is therefore next to impossible. For this reason the capacitors are kept out of the liquid nitrogen, and a cable is used to connect the coil and the capacitor. For convenience in tuning, a Jennings variable vacuum capacitor (rated at 10 kV) was used.

The probe and dewar are both supported by a wooden frame built around the magnet. A pointer and a protractor placed on the wooden frame make it possible to do orientation studies.

The RF cable is highly magnetic at liquid nitrogen temperature, causing an inhomogeneous broadening of the NMR line when it is too close to the sample. For this reason the cable is not run all the way to the sample, but is kept approximately 35 cm from the sample.

Figure 2. Liquid Nitrogen Probe

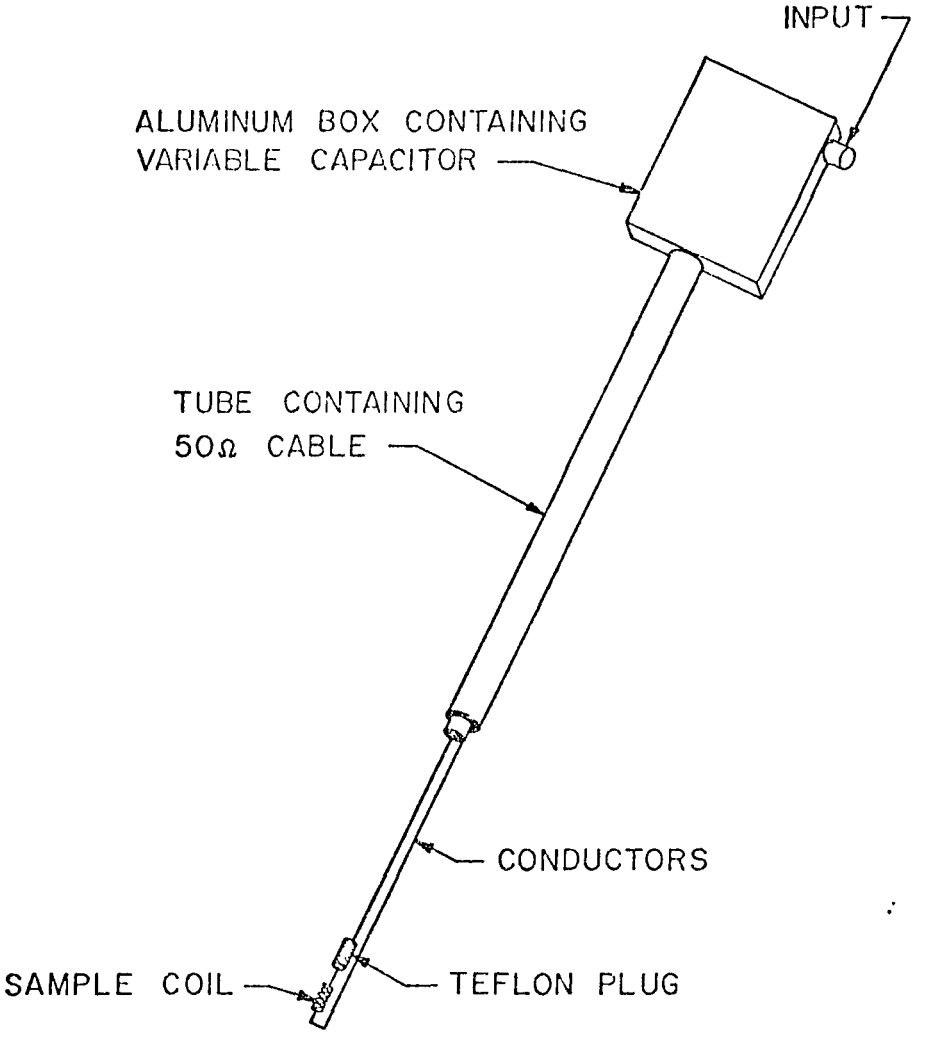
INPUT
ALUMINUM BOX CONTAINING
VARIABLE CAPACITOR
TUBE CONTAINING
50Ω CABLE
CONDUCTORS
SAMPLE COIL
TEFLON PLUG

The best Q, and therefore the best signal, for the circuit can be produced by winding a coil with the right inductance and parallel capacitance so that when tuned with a capacitor it gives an impedance of 50Ω at the resonance frequency. This is normally accomplished by winding a coil that is too long, then removing turns until the coil can be tuned to 50Ω at the NMR resonance frequency. In this probe, the parallel capacitance of the cable between the coil and capacitor plays an important part in the tuning. Since the cable runs between room temperature and liquid nitrogen temperature, the parallel capacitance tends to drift with time. This causes considerable drift in the tuning of the whole circuit. When the tuning changes, so does the phase of the signal and the length of a 90° pulse. The instability of these two factors makes it impossible to constantly reproduce the same signal, which is required in order to signal average. To reduce this problem a resistor is placed in series with the coil and the capacitor, and the circuit is retuned to 50Ω . This resistor lowers the Q and makes the tuning less dependent on the parallel capacitance of the cable. The typical resistance used is approximately 20Ω .

C. Tektronix Interface

To facilitate the transfer of data from the spectrometer to the William and Mary Computer Center's IBM 370, we built an interface between the Digital Equipment PDP-8/e and a Tektronix 4013-1 computer terminal, which in turn is connected to the IBM 370. The output from a previously designed tape drive interface is used as the output from the PDP-8/e. The new interface converts this output to an appropriate form for the bus of the Tektronix terminal.

The data is converted into ASCII code by the PDP-8/e. Along with the numeric characters, a carriage return is supplied by the PDP-8/e. For all these characters Bit 7 is always low; therefore, it is tied low on the interface. The other 6 bits of the ASCII representation along with a "Step/Write" signal, come from the PDP-8/e on 7 different data lines. Returning to the PDP-8/e is a "Busy" signal, which places the PDP-8/e in a hold loop until the terminal is ready to process another character. The interface is activated by the "Step/Write" signal which tells the interface to process the data on the data lines.

The interface is also controlled by three signals on the Tektronix bus, $\overline{\text{CPUNT}}$, $\overline{\text{CBUSY}}$, and a 614 kHz clock. When $\overline{\text{CPUNT}}$ and $\overline{\text{CBUSY}}$ are low, it indicates the terminal is busy either sending or receiving and places the interface in a hold mode. The 614 kHz clock controls the timing of the outputs of the interface to the bus, making sure they appear at the right time. Outputs of the interface to the bus are $\overline{\text{Bits}}$ 1-7 of the ASCII coded character and CSTROBE. CSTROBE indicates to the terminal that the data on the bus is to be processed and sent to the IBM 370.

Figure 3. Interface from PDP-8/e to Tektronix 4013-1 Bus

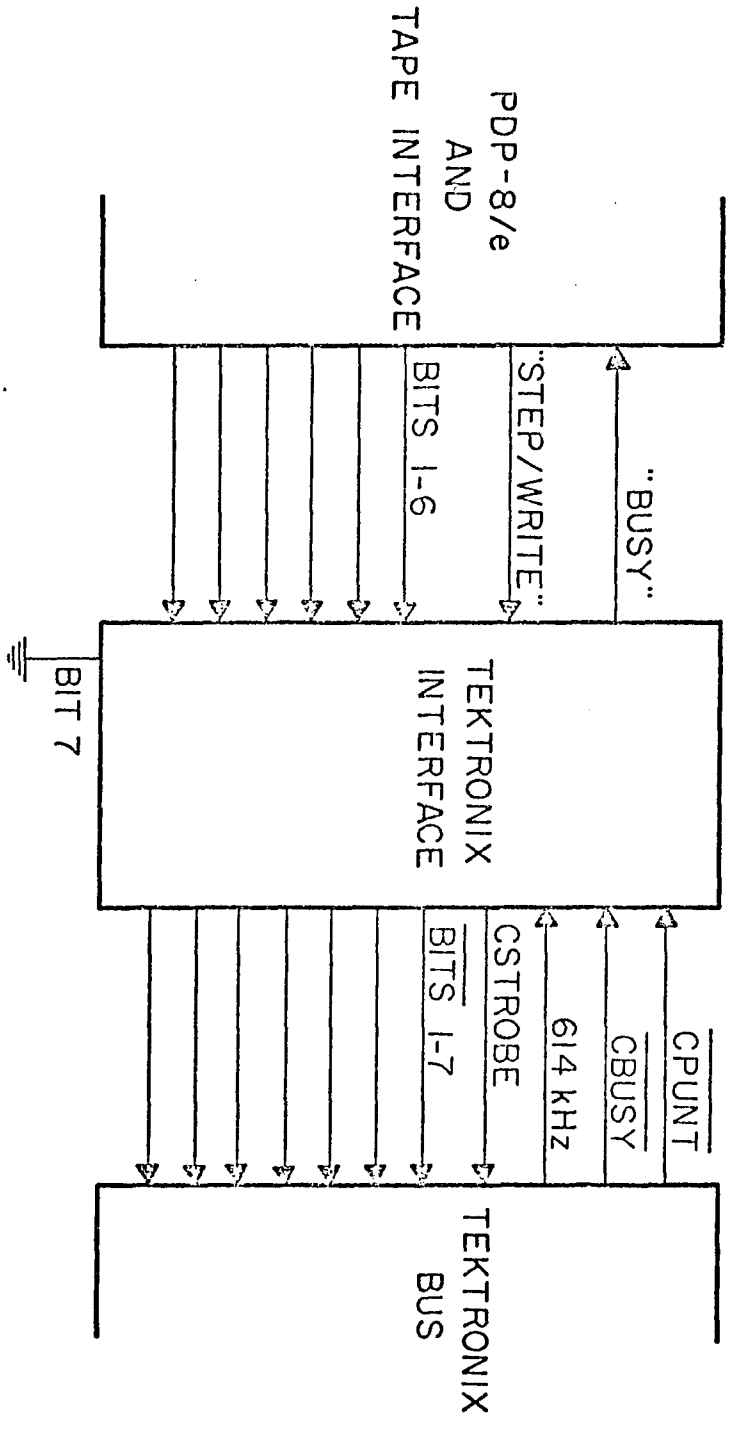
PDP-8/e
AND
TAPE INTERFACE
"STEP/WRITE"
BITS 1-6
"BUSY"
BIT 7
TEKTRONIX
INTERFACE
CSTROBE
BITS 1-7
614 kHz
CBUSY
CPUNT
TEKTRONIX
BUS

III. THEORY

Recently theories of the change of lineshape arising from point charged defects[6,7,11] have been developed. These theories consider a dielectric medium in which the electric field gradient varies as r^{-n}, where n is an integer and r is the distance from a charged defect. For this case, Fedders finds the change in the free induction decay to be an exponential function of $t^{3/n}$, where t is the time following a 90° pulse. For a semiconductor, however, the charged defects are screened by the free carriers present. The result is an electric field, and therefore an electric field gradient, that decreases with a separation from the defect site faster than the unscreened field. This changes the form of the free induction decay. The following discussion is a modification of the previous results to include the effect of this screening for a spin 3/2 nuclei in a lattice with zinc-blende structure.

Fedders examines the case of randomly spaced point defects with small concentrations (i.e., the number of defects is small compared to the number of lattice sites). He further constrains the problem to the case where the quadrupole shift is small compared to the width of the Zeeman levels. As a result of these assumptions, the problem can be reduced to one of treating the effect of one point defect on all the surrounding nuclei. Fedders' expression for the modulation of the free induction decay is

$$Q(t) = e^{-\rho_d I(t)}, \tag{1}$$

where

$$I(t) = \int d^3r \left(1 - e^{-i\bar{\omega}(\vec{r})t}\right), \tag{2}$$

and ρ_d is the density of point defects. $\bar{\omega}(\vec{r})$ is the quadrupole frequency shift of the resonance of the nucleus located at $\vec{r}$, resulting from a point defect located at the origin. The quadrupole modified decay shape (F(t)) is then given by the expression

$$F(t) = Q(t)\,V(t), \tag{3}$$

where V(t) is the decay shape with no quadrupole broadening.

The first order 3/2 to 1/2 transition quadrupole shift of a spin 3/2 nucleus is[12]

$$\bar{\omega}(\vec{r}) = 2A \sum_{ij}{}' V_{ij}(\vec{r})\,(3\gamma_i\gamma_j - \delta_{ij}), \tag{4}$$

where $V_{ij}(\vec{r})$ is the electric field gradient at $\vec{r}$, γ_i and γ_j are the direction cosines of the Zeeman field with respect to the lattice axes, and the constant A is given by

$$A = eQ/[4I(2I-1)]\hbar, \tag{5}$$

where Q is the quadrupole moment of the nuclear spin I.

For the zinc-blende structure, the electric field gradient induced by an external electric field is given by[13]

$$V_{ij}(\vec{r}) = -R_{14}\,\epsilon \sum_k \delta_{ijk} E_k(\vec{r}), \tag{6}$$

where $E_k(\vec{r})$ is the k th (k = x,y,z) component of the electric field at the nucleus, ϵ is the dielectric constant, R_{14} is a constant dependent on the particular crystal and atom of interest, and δ_{ijk} is 1 for i, j and k all different and zero otherwise.

A screened Coulomb potential is given by the expression

$$\phi(r) = \frac{e^*}{\epsilon r} e^{-\lambda r}, \tag{7}$$

where λ is the screening constant, and e^* is the effective charge of the point defect, i.e., the difference between the actual charge of the defect and the charge a host atom would have at that location. Since the electric field is the negative of the gradient of the potential, the screened electric field is given by

$$E(\vec{r}) = \frac{e^*}{\epsilon r^2}(1+\lambda r) e^{-\lambda r} \hat{r}$$
$$\equiv \frac{e^*}{\epsilon} h(r) \hat{r}. \tag{8}$$

Using equations (4), (6) and (8), one can show that the resulting frequency shift of the transition is

$$\bar{\omega}(\vec{r}) = 2A R_{14} e^* \sum_{i,j,k}' (3\gamma_i \gamma_j - \delta_{ij}) \delta_{ijk} \Omega_k h(r), \tag{9}$$

where Ω_k is the direction cosine between the electric field at the nucleus and the k direction. This can be simplified to the result

$$\bar{\omega}(\vec{r}) = \alpha \cos\psi \quad h(r), \tag{10}$$

where

$$\alpha = 12 A R_{14} e^* (\gamma_x^2 \gamma_y^2 + \gamma_y^2 \gamma_z^2 + \gamma_z^2 \gamma_x^2)^{1/2}, \tag{11}$$

and ψ is the angle between the electric field and the vector denoted by the coordinates ($\gamma_x \gamma_y$, $\gamma_y \gamma_z$, $\gamma_z \gamma_x$). The angle ψ occurs in a configuration average below (Eq. 13), so it need not be specified in more detail. If the crystal is rotated about the (110) axis that is kept perpendicular to the Zeeman field, α reduces to

$$\alpha = 6 A R_{14} e^* (4\cos^2\theta - 3\cos^4\theta)^{1/2}, \tag{12}$$

where θ is the angle between a (110) axis in the plane of rotation and the Zeeman field.

To solve for the form of the modulation function Q(t), $\vec{\omega}(\vec{r})$ from Eq. (10) is substituted into Eq. (2) to give

$$I(t) = \int d^3r \left(1 - e^{-i\alpha (\cos\psi)\, h(r) t}\right). \tag{13}$$

Integrating over the angular part gives

$$\begin{aligned} I(t) &= 4\pi \int_0^\infty dr\, r^2 \left(1 - \frac{\sin(\alpha\, h(r) t)}{\alpha\, h(r) t}\right) \\ &= 4\pi \int_0^\infty dr\, r^2 \left(1 - \frac{\sin\left(\tfrac{1}{2}(r\lambda+1) e^{-\lambda r} \alpha t\right)}{\tfrac{1}{2}(r\lambda+1) e^{-\lambda r} \alpha t}\right). \end{aligned} \tag{14}$$

By making the substitutions $r = x\sqrt{\alpha t}$ and $\lambda\sqrt{\alpha t} = q$ this integral is transformed to

$$I(t) = 4\pi (\alpha t)^{3/2} f(q), \tag{15}$$

where

$$f(q) \equiv \int_0^\infty dx\, x^2 \left(1 - \frac{\sin\left(\tfrac{1}{2} (qx+1) e^{-qx}\right)}{\tfrac{1}{2} (qx+1) e^{-qx}}\right). \tag{16}$$

The function f(q) is evaluated numerically. The screening constant is related to the charge carrier concentration through the Debye screening constant formula

$$\lambda = \left[\frac{4\pi e^2 n_0}{\epsilon k T}\right]^{1/2}, \tag{17}$$

where n_0 is the charge carrier concentration, T is the absolute temperature and k is the Boltzmann constant. Therefore, q as a function of charge carrier concentration and time is

$$\begin{aligned} q &= \left[\frac{4\pi e^2 \alpha}{\epsilon k T}\right]^{1/2} (n_0 t)^{1/2} \\ &\equiv \beta (n_0 t)^{1/2}. \end{aligned} \tag{18}$$

The second equality in Eq. (18) defines β . Using Eqs. (1), (15) and (18), the modulation function for the 3/2 to 1/2 transition decay shape is given by

$$Q(t) = e^{-\beta_d (4\pi)(\alpha t)^{3/2} \int (\beta (n_0 t)^{1/2})} , \tag{19}$$

where

$$\alpha = \frac{eQ}{2\hbar} R_{14} e^{*} \left(4\cos^2\theta - 3\cos^4\theta\right)^{1/2} . \tag{20}$$

Q(t) for different values of defect density and carrier concentrations are shown in Figs. 4, 5 and 6.

As can be seen from those figures Q(t) depends much more sensitively on defect density than it depends on carrier concentration. There is, however, a noticeable effect from the charge carriers, when the carrier concentration becomes comparable to the defect density. For the carrier concentration equal to zero, f(q) is given by

$$f(0) = \int_0^\infty dx\, x^2 \left(1 - \frac{\sin(1/x^2)}{1/x^2}\right) \tag{21}$$
$$= \frac{2\sqrt{2\pi}}{15} .$$

Therefore, for no free charge carriers, I(t) is given by

$$I(t) = \frac{8\pi\sqrt{2\pi}}{15} (\alpha t)^{3/2} , \tag{22}$$

which is the I(t) found by Fedders[6] and by Cueman, et al.[7]

The change in the 3/2 to 1/2 transition decay shape as a function of defect density and carrier concentration is given by Q(t). To first order the 1/2 to -1/2 transitions is unaffected by the quadrupole Hamiltonian. The composite shape is the sum of the contributions from the 3/2 to 1/2, 1/2 to -1/2 and -1/2 to -3/2 transitions, normalized by their relative intensities. The contribution from the 3/2 to 1/2, and

Figure 4. Q(t) as a function of defect density

Isotope -Ga^{71} $\theta = 35^{\circ}$ carrier concentration = 0

A - $\rho_d = 10^{13} cm^{-3}$

B - $\rho_d = 10^{14} cm^{-3}$

C - $\rho_d = 10^{15} cm^{-3}$

D - $\rho_d = 5 \times 10^{15} cm^{-3}$

E - $\rho_d = 10^{16} cm^{-3}$

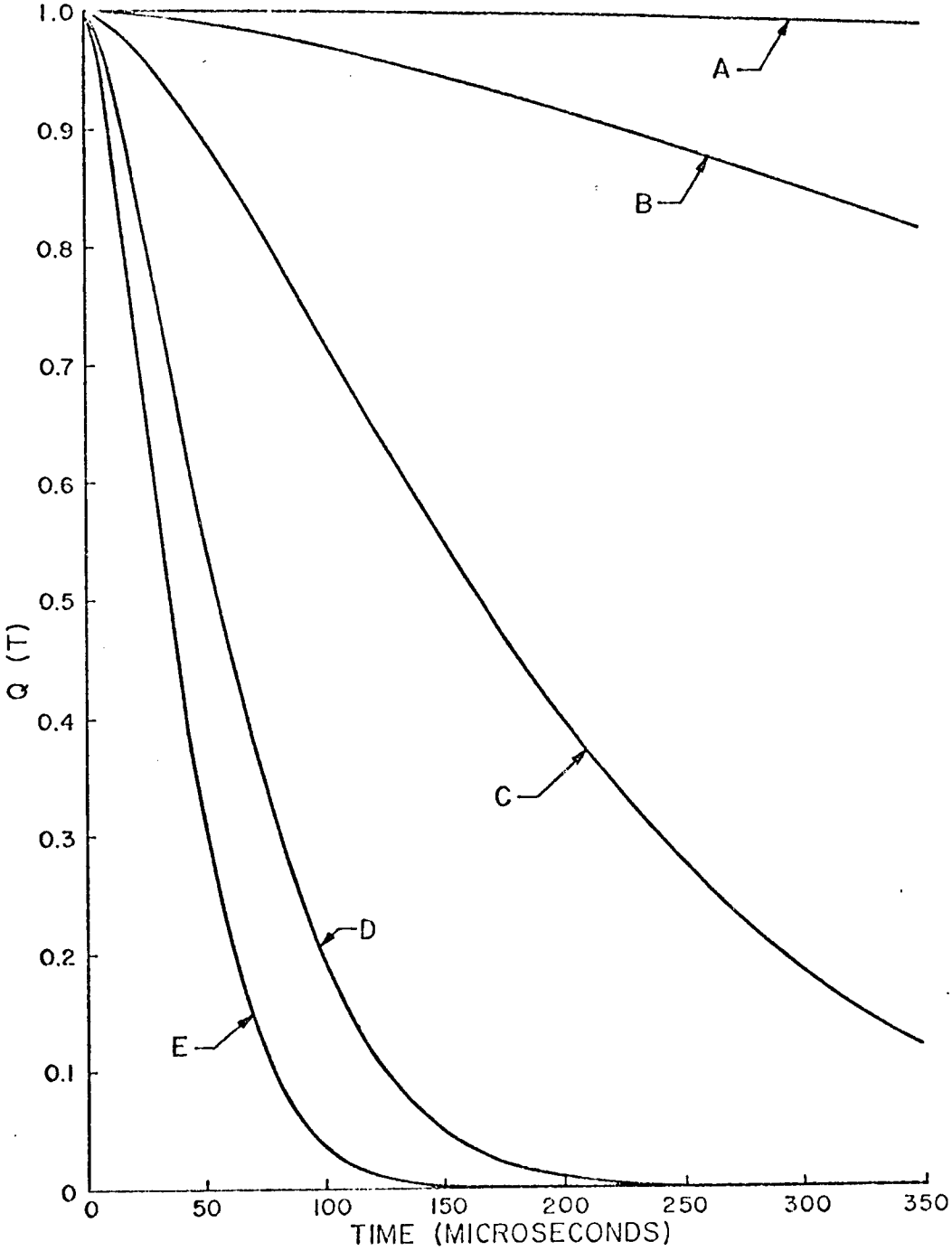
1.0
0.9
0.8
0.7
0.6
0.5
0.4
0.3
0.2
0.1
0
Q (T)
A
B
C
D
E
0
50
100
150
200
250
300
350
TIME (MICROSECONDS)

Figure 5. Q(t) as a function of carrier concentration

Isotope $-Ga^{71}$ $\theta = 35^{o}$ $\rho_d = 10^{15} cm^{-3}$

A - $n_o = 0$

B - $n_o = 10^{14} cm^{-3}$

C - $n_o = 10^{15} cm^{-3}$

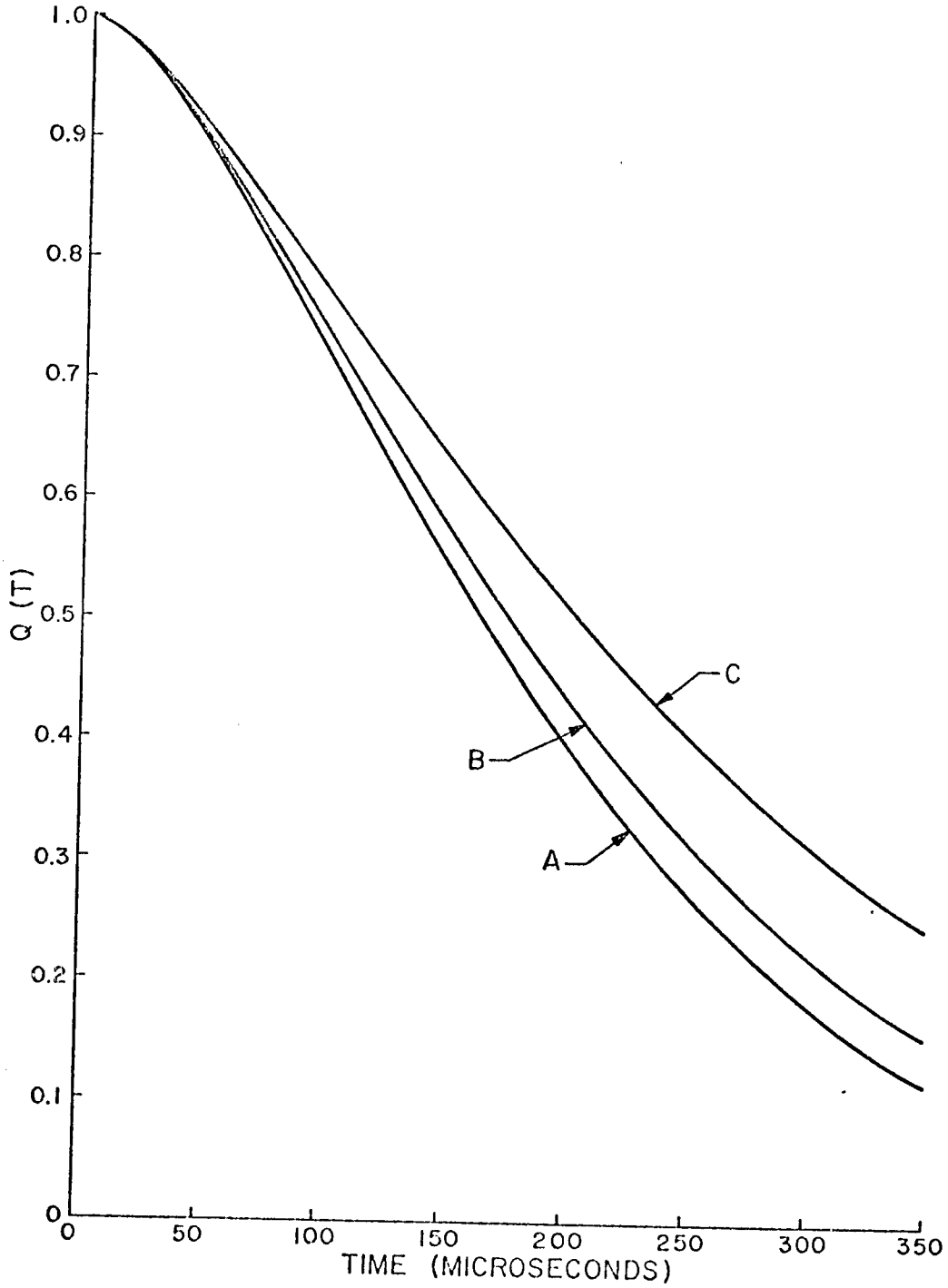
1.0
0.9
0.8
0.7
0.6
0.5
0.4
0.3
0.2
0.1
0
Q (T)
0
50
100
150
200
250
300
350
TIME (MICROSECONDS)
A
B
C

Figure 6. Q(t) as a function of carrier concentration

Isotope -Ga^{71} $\theta = 35^{o}$ $\rho_d = 5 \times 10^{15} cm^{-3}$

A - $n_o = 0$

B - $n_o = 10^{14} cm^{-3}$

C - $n_o = 10^{15} cm^{-3}$

D - $n_o = 5 \times 10^{15} cm^{-3}$

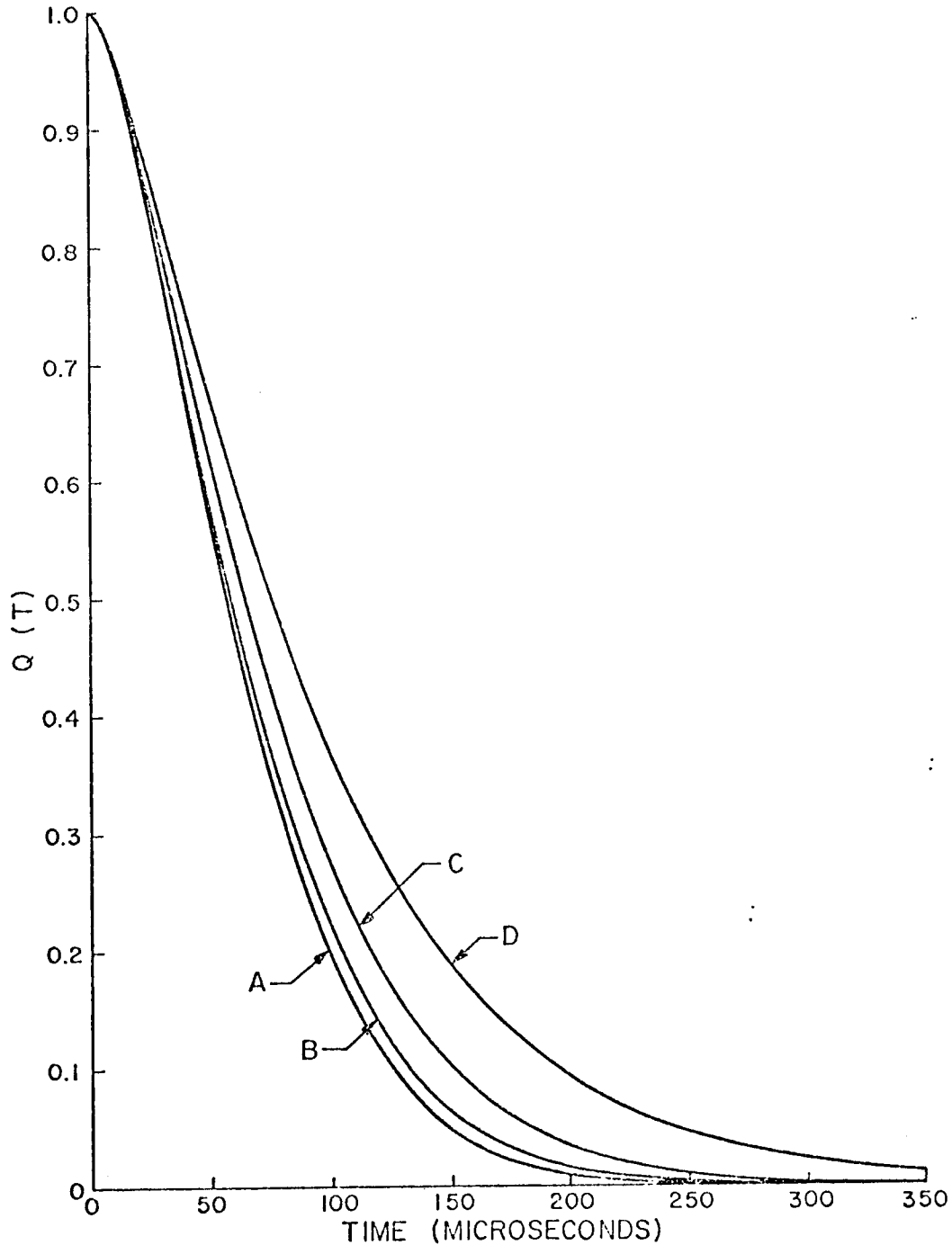
1.0
0.9
0.8
0.7
0.6
0.5
0.4
0.3
0.2
0.1
0
Q (T)
0
50
100
150
200
250
300
350
TIME (MICROSECONDS)
A
B
C
D

-1/2 to -3/2 transitions is given by Eq. (3). The contribution of the 1/2 to -1/2 transition is just the unbroadened decay shape, V(t). Therefore, the decay shape seen is

$$F(t) = 0.4\, V(t) + 0.6\, Q(t)\, V(t), \qquad (23)$$

where 0.4 and 0.6 are the relative intensities of the transitions.

IV. EXPERIMENTAL PROCEDURE

A. Reduction of the Piezoelectric Response

In pulsed NMR investigations of high purity GaAs, the resonance signal is obscured by two effects. The first effect is the usual random noise associated with the circuit. Signal averaging enhances the signal with respect to this noise. The second effect is the piezoelectric response of the sample, which is found to be repetitive in shape with each pulse. It is not possible, therefore, to enhance the signal with respect to the piezoelectric response by simply signal averaging.

Various attempts have been made to reduce the piezoelectric response with respect to the NMR signal.[8] One method is to wrap the sample in mylar to form a Faraday shield around it, which tends to decouple the piezoelectric response from the receiver coil. Another is to place the sample in a viscous liquid that tends to damp out the piezoelectric response of the crystal. While these methods reduce the piezoelectric response relative to the NMR signal, they do not completely eliminate it.

Cueman[9] found a way to reduce piezoelectric interference which makes use of an observation that the piezoelectric response of the crystal is dependent on the phase and length of the RF pulse. Knowing this, he was able to increase the signal relative to the piezoelectric response. His method employed two pulses, one that produced the NMR signal with the piezoelectric response superimposed on it, but

the other produced only the piezoelectric response of the crystal. The second pulse is 180° out of phase with the first pulse. The piezoelectric response after this second pulse has nearly the same shape as the piezoelectric response after the first pulse, but is inverted. When the signals from the two pulses are added, the piezoelectric responses are approximately cancelled. This method still does not completely eliminate the unwanted signal. It has the additional problem of decreasing the signal to random noise ratio of the averaged signal, since one of the responses contains no NMR signal.

From the experimental observation that the piezoelectric response depends only on the phase and length of the RF pulse and not on the NMR signal, on which it is superimposed, a new pulse sequence was found for increasing the averaged signal to piezoelectric response ratio. It is possible to use it in cases where the spin-lattice relaxation time T_1 is long compared to the spin-spin relaxation time, T_2. The pulse sequence, shown in Fig. 7, begins with a 90° pulse. The signal produced by the 90° pulse contains the NMR signal with the piezoelectric response superimposed on it. After a time T_1, the magnetization has realigned with the external magnetic field. A 180° pulse then rotates the magnetization of the sample antiparallel to the magnetic field. When this pulse is followed by a 90° pulse, the ensuing signal will be an inverted NMR signal (since the magnetization began antiparallel to the magnetic field), but the piezoelectric response superimposed on it is not inverted since it depends only on the phase and length of the pulse which is the same as that of the first 90° pulse. If this signal is

Figure 7. Pulse sequence for reduction of piezoelectric response

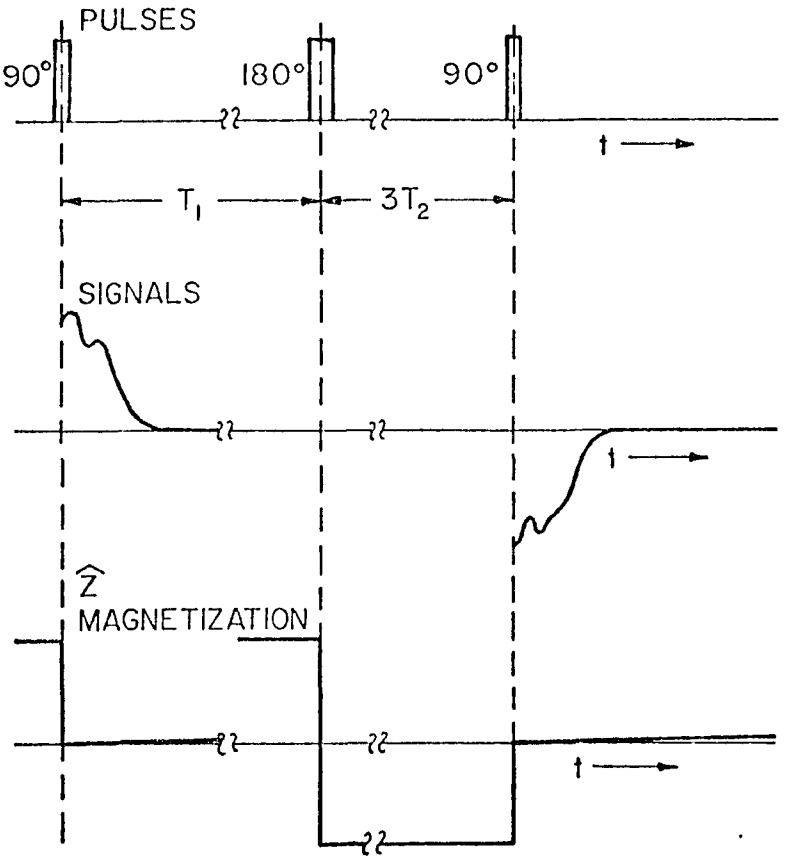
PULSES
90°
180°
90°
t
T_1
$3T_2$
SIGNALS
t
$\hat{Z}$
MAGNETIZATION
t

subtracted from the signal following the first pulse, the piezoelectric response will then cancel leaving only the sum of the two NMR signals. After waiting another time T_1 for the magnetization to realign with the magnetic field, the pulse sequence begins again.

A time delay of 3 or 4 T_2's is employed between the application of the 180° pulse and the second 90° pulse. This allows any off-diagonal components of the magnetization introduced by 180° pulse to decay to zero.

The large increase of the signal to piezoelectric response ratio can be seen in Fig. 8. Experimental observations clearly indicate this method produces a much larger increase of this ratio than the previous method. In addition, this method, unlike the others, causes no decrease in the averaged signal to random noise ratio. Except for the loss of magnetization caused by T_1 processes, during the time interval between the 180° pulse and the 90° pulse, the magnitude of the free induction decay after the two 90° pulses are equal. The estimated worse case gives this loss as less than 1%, therefore, since the magnitudes are nearly equal, the signal to random noise ratio is the same as if there were no 180° pulse applied. This method then greatly reduces the distortion of the averaged lineshape resulting from the piezoelectric response of the crystal without reducing the signal to random noise ratio.

Figure 8. Comparison of free induction decays using and not using the new method for reduction of piezoelectric response

A - FID not using new method

B - FID using new method

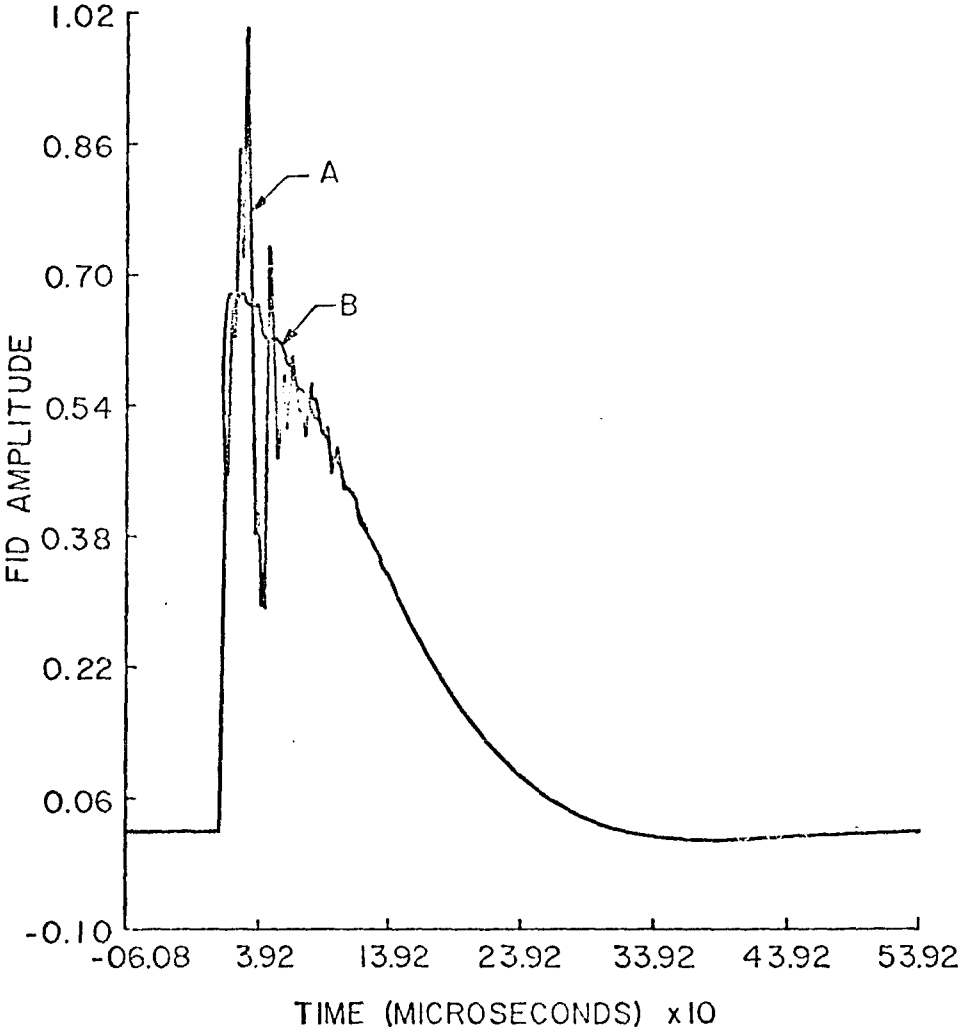
1.02
0.86
0.70
0.54
0.38
0.22
0.06
-0.10
FID AMPLITUDE
A
B
-06.08
3.92
13.92
23.92
33.92
43.92
53.92
TIME (MICROSECONDS) x10

B. Measurement of the Defect Density and Carrier Concentration

The basic objective of this experiment is to use the theory, derived in Chapter III, to deduce the change in the defect density and carrier concentration of GaAs samples. To facilitate the data reduction, a procedure for examining the decay shape was established in the beginning of the experiment and adhered to as much as possible thereafter.

The decay shape F(t) of the free induction decay found in Chapter III is

$$F(t) = (0.4 + 0.6\, Q(t))\, V(t) \tag{24}$$

where

$$Q(t) = e^{-\rho_s (4\pi) (\alpha t)^{3/2} f(\beta (n_s t)^{1/2})} \tag{25}$$

In practice, the decay shape with no quadrupole broadening (V(t)) cannot be measured directly since perfect samples are unavailable. Therefore, the defect density and the carrier concentration of the sample being examined is determined by comparing its free induction decay to the free induction decay of a sample for which the defect density and carrier concentration are known. This is done by solving Eq. (24) for both signals simultaneously to give

$$F_u(t) = F_k(t)\, A \left(\frac{0.4 + 0.6\, e^{-(\rho_u (4\pi) (\alpha t)^{3/2} f(\beta (n_u t)^{1/2}))}}{0.4 + 0.6\, e^{-(\rho_k (4\pi) (\alpha t)^{3/2} f(\beta (n_k t)^{1/2}))}} \right) \tag{26}$$

where ρ_u, n_u and $F_u(t)$ are the defect density, the carrier concentration and the free induction decay for the sample for which the defect density and carrier concentration are known. ρ_k, n_k and $F_k(t)$

are the defect density, carrier concentration and free induction decay for the sample for which the defect density and carrier concentration are known. The constant A is introduced for normalization. Eq. (26) applies if the two samples have the same orientation in the magnetic field. In addition to an orientation dependence of the perfect crystal free induction decay V(t) caused by the dipole and pseudodipolar broadening, there is also an orientation dependence of the quadrupole broadening which enters through the parameters α and β defined in Eqs. (11) and (18). Fitting the data to this orientation dependence is an important aspect of the method used to extract the defect density and carrier concentration from the measurements for they are calculated by doing an average over the different orientations.

Ideally, one would like to begin an orientation study of the free induction decays of the sample by placing the sample with one (110) axis perpendicular to the magnetic field and another (110) axis parallel to the magnetic field. With our experimental arrangement it is not possible to do this exactly. The original orientation of the crystal is invariably offset slightly from this ideal condition and the results are sensitive to small deviations from the ideal arrangement. The size of this offset was found by doing a moments analysis as described by Hester.[8] The offset found from the moments analysis was used to determine the absolute orientation of the sample in the magnetic field for all subsequent analysis. A free induction decay was recorded for the sample in this original position and for every 10 degrees of rotation

about the (110) axis oriented perpendicular to the magnetic field, until the crystal had been rotated 110°. Free induction decays were recorded also for rotations of 35°, 85° and 95° with respect to the original orientation.

For these orientations the angular dependence of α and β are given in Chapter III as $g^{3/4}(\theta)$ and $g^{1/4}(\theta)$ respectively, where $g(\theta)$ is given by the expression

$$g(\theta)=0.75(4\cos^2\theta-3\cos^4\theta), \tag{27}$$

and θ is the angle between the magnetic field and the (110) axis that is in the plane of rotation. As can be seen from Fig. 9, $g(\theta)$ peaks for θ approximately equal to 35° and drops to zero for θ equal to 90°. Therefore, the quadrupole broadening varies from orientation to orientation, becoming most significant when $\theta \approx$ 35° and approaching zero as θ approaches 90°.

To find the defect density and the carrier concentration of the sample, the free induction decays for θ's varying between 0° and 50° were fit using Eq. (26). The decays were fit using a three parameter least-squares fitting routine. The parameters used in the fitting routine were the square root of the carrier concentration, the defect density and the normalization constant. Each fit, for each free induction decay at the different orientations, produced a value for the carrier concentration and defect density. These values are averaged to give the defect densities, the carrier concentrations and their respective standard deviations.

Figure 9. Angular dependence of $g(\theta)$

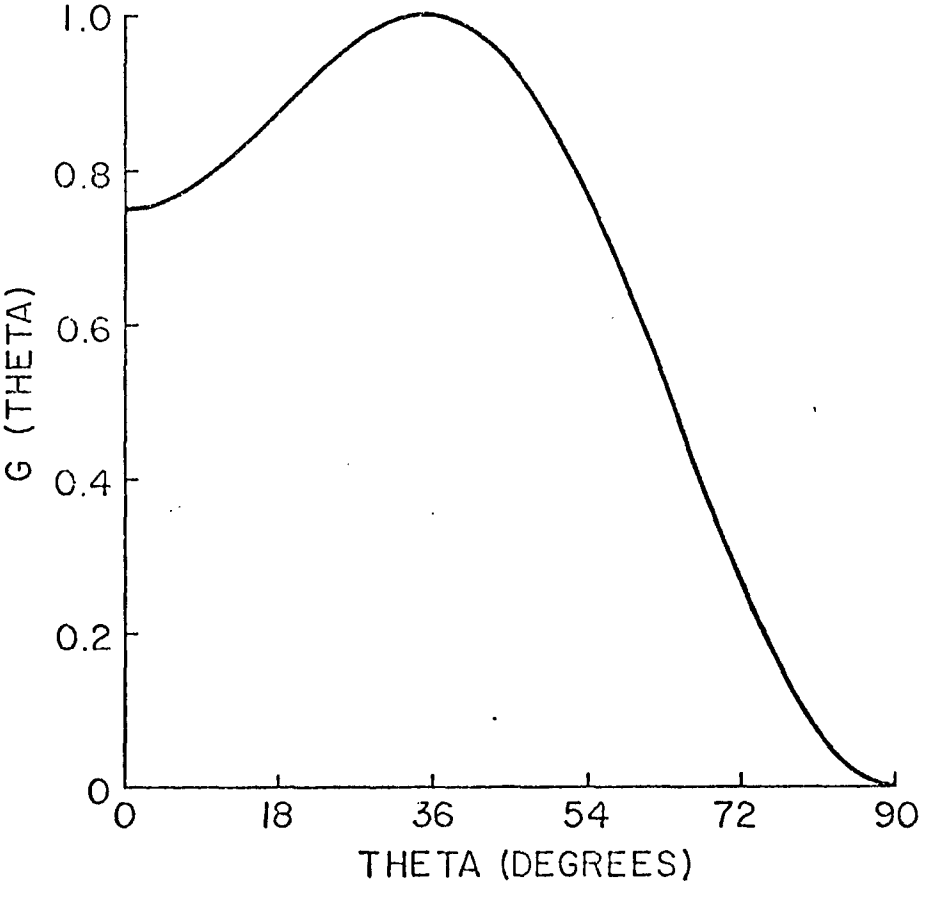
1.0
0.8
0.6
0.4
0.2
0
G (THETA)
0
18
36
54
72
90
THETA (DEGREES)

The free induction decays for orientations $\theta \geq 60^{\circ}$ were fit also. These fits systematically gave values for the defect density that varied by two or three standard deviations from the average defect density obtained by fitting the data for orientations with the range $0^{\circ} \leq \theta \leq 50^{\circ}$. One would expect the information deduced from orientations $\theta \geq 60^{\circ}$ to be less reliable since it is evident from Fig. 9 that $g(\theta)$ becomes small for these values. Therefore, as the quadrupole broadening becomes smaller, other small changes in the decay shape resulting from orientation errors or magnetic field drift would be mistaken for a large change in the defect density. For this reason the data for $\theta \geq 60^{\circ}$ is not used to calculate the defect density and carrier concentration.

To determine the range of carrier concentrations that can be accurately measured by this technique, decay shapes were simulated using Eq. (26) for different carrier concentrations and defect densities. These simulated decay shapes were then fit following the procedure described above. The method produces an accurate value for the carrier concentration only if the carrier concentration is 10^{14}cm^{-3} or greater. We are dealing with defect densities on the order of 10^{15}cm^{-3}. Fitting of these simulated decay shapes also indicate that if the carrier concentration falls below 10^{14}cm^{-3}, the defect density can be found just as accurately from a two parameter least-squares fit of the free induction decays (see Eq. (26)) with the carrier concentrations set equal to zero. Therefore, when the carrier concentration was known to be less than 10^{14}cm^{-3}, this two parameter fit was used to find the defect density.

As mentioned before, Eq. (26) is correct only if the two samples have the same orientations in the magnetic field. To approximate this condition as closely as possible, free induction decays were recorded for every 2°, for θ ranging from -10° to 80°, prior to irradiation. This established the data base for $F_k(t)$. Thus it was possible to match the orientations of the two samples to within 1°. The defect density of the starting material was known from an analysis done by Cueman.[9] The carrier concentration was given by the manufacturer (Monsanto) as $2.4 \times 10^{11} cm^{-3}$.

Finally, to apply Eq. (26) to GaAs, it is necessary to know the value of ϵ, and Q and R_{14} for each of the isotopes. The values of these parameters along with their source references are given in Table I.

TABLE I

Dielectric constant for GaAs = 12.56 ± 0.04[a]

	As^{75}	Ga^{69}	Ga^{71}
Quadrupole moment (barns)	0.29[b]	0.19[c]	0.12[c]
$R_{14}(10^{10}cm^{-1})$	3.16[d]	2.85[d]	2.85[d]

[a]G. E. Stillman, D. M. Larsen, C. M. Wolfe and R. C. Brandt, Solid State Commun. 9, 2245 (1971)

[b]V. S. Korolkov and A. G. Makhanek, Opt. Spectry. USSR (English Transl.) 12, 87 (1962)

[c]G. F. Koster, Phys. Rev. 86, 148 (1952)

[d]K. A. Dumas, unpublished Ph.D. dissertation, College of William and Mary (1978)

V. EXPERIMENT

A. Gamma Ray Damage of Gallium Arsenide

In the wake of a theory giving the variation of the NMR lineshape of a GaAs crystal as a function of charged defect density, Cueman began a study of the number of charged defects created by gamma irradiations. He gamma irradiated a GaAs sample twice, and measured the defect density after each irradiation. Examining only the Ga^{71} resonance, he determined that the three defect densities followed a linear dependence on fluence.

The irradiations and measurements were continued subsequent to Cueman's experiment. However, the measurements of the defect density of several different slices of the ingot from which Cueman took his sample, showed the defect density varried from slice to slice. Thus, his data were reanalyzed for an important assumption of his analysis was that all slices of the ingot had the same defect density. The defect densities after each irradiation, found by reanalysis of Cueman's data and by the analysis of subsequent data, are given in Table II.

The data in Table II shows a definite increase in the defect density of the sample with each subsequent irradiation, until the last one where we find a sharp decrease. For a linear damage rate, the quantity $\Delta\rho_d / \Delta N_\gamma$ should be constant. This obviously is untrue, since it became negative on the last irradiation. This disagreed with the observation of Cueman.

TABLE II

Fluence (N_γ)(cm^{-2})	Defect density (ρ_d)($10^{14} cm^{-3}$)	$\Delta\rho_d/\Delta N_\gamma$($cm^{-1}$)
0	$0.9 - 2.0^{\psi}$	-
1.41×10^{16}	1.6 ± 0.1	?*
2.72×10^{16}	2.9 ± 0.2	0.009 ± 0.002
4.03×10^{16}	3.5 ± 0.2	0.004 ± 0.002
5.34×10^{11}	1.7 ± 0.1	-0.013 ± 0.002

ψ - initial defect density of sample unknown - range of defect densities on slices to each side of sample given

* - initial defect density unknown

Experimental results: Defect densities of gamma irradiated sample

How can the behavior of this apparent defect density be explained? Either the measurement method is failing, as a result of certain approximations of the theory being incorrect for this crystal; or the apparent changes are just a consequence of systematic errors in the measurements and the early data reduction procedure, and there is no real change in the defect density of the sample. We now believe the second explanation to be true. However, other explanations were investigated. Since these do, in some circumestnaces, impose limits on the method, two will be presented next.

The first explanation explored was that the quadrupole broadening increased to the point where one of the basic assumptions of the theory,

$$[\mathcal{H}_Q, \mathcal{H}] = 0, \tag{28}$$

failed, where $\mathcal{H}_Q$ is the Hamiltonian for the quadrupole interaction, and $\mathcal{H}$ is the total Hamiltonian for the nuclei. This possibility was tested by repeating the experiment and examining all three isotopes, instead of just one. Since the quadrupole broadening is proportional to the product of R_{14} (a constant that relates the electric field gradient to the electric field, for GaAs) and the quadrupole moment, and this product varies from isotopes to isotope, the approximation (Eq. (28)) breaks down for the three isotopes at three different densities. The defect densities, for which Eq. (28) fails, are estimated to be 10, 5 and 2 x 10^{14}cm^{-3} for Ga^{71}, Ga^{69} and As^{75}, respectively.[7]

If the resonances from all three isotopes are examined between each irradiation and they appear to give a decrease in the damage rate at the three different prescribed levels of defect density, the behavior could be ascribed to the failure of Eq. (28). There is no simple correction to the theory to compensate quantitatively for the failure of Eq. (28). As we shall demonstrate presently no evidence for the failure of Eq. (28) was found.

A second possible explanation for the odd behavior of the data is that sufficient free charge carriers were created by the irradiations to screen the electric field created by the charged defects. This would account for the apparent decrease in the charge defect density for the highest dose. This possibility can also be tested experimentally by comparing the decay shapes measured at room temperature and liquid nitrogen temperature. The Debye screening length, given by

$$l = \left[\frac{\epsilon k T}{4\pi e^2 n_o}\right]^{1/2} \tag{29}$$

depends directly on the square root of the temperature and indirectly depends on it through the temperature dependence of n_o , the carrier concentration. If the carrier ionization energy is sufficiently large then n_o will change considerably between room and liquid nitrogen temperature so the effect on l will be amplified. However, even if the carriers have shallow ionization energies so n_o remains almost constant as the temperature is lowered, the change in l of about a factor of two arising from the direct temperature dependence should still be easy to detect. Therefore, if the carrier concentration is large

enough to affect the NMR signal by screening the electric field, the signal should change as the temperature of the sample is reduced from room temperature to liquid nitrogen temperature. Thus, one should be able to tell if there is an effect on the lineshape due to screening. The effect of screening can be incorporated quantitatively into the theory as shown in Chapter III. This makes it possible by measuring the carrier concentration by another method to see if it should affect the decay shape.

To explore these two possibilities, the experiment was repeated, with another slice of the same ingot. Also, changes were made to improve the information collected. These included examining the resonances of all three isotopes after each irradiation, and measuring the decay shapes of the resonances when the sample was at room temperature and liquid nitrogen temperature. In addition, a smaller fluence of gammas was used for each irradiation of the sample to better track the effect seen in the previous experiment. The fluence of gammas per step was increased as it became appropriate.

The defect density measured after each irradiation is given in Table III. The errors quoted include only statistical errors associated with the fitting procedure and do not reflect inaccuracies caused by sample alignment or other systematic errors. There is no systematic change in the charged defect density of the sample with the irradiation by gamma rays. To within the experimental accuracy of this measurement the defect density remains constant at $1.54 \pm 0.06 \times 10^{14} cm^{-3}$,

TABLE III

Total Fluence (cm^{-2})	Defect Density as Measured by Ga^{69}	Ga^{71}	As^{75}	($10^{14} cm^{-2}$)
0			1.5±0.1	
1.87×10^{16}	1.5±0.1	1.4±0.1	1.6±0.1	
0.375×10^{16}	1.6±0.1	1.4±0.1	1.6±0.1	
0.563×10^{16}	1.6±0.1	1.5±0.1	1.6±0.1	
0.750×10^{16}	1.6±0.1	1.5±0.1	1.6±0.1	
0.938×10^{16}	1.4±0.1	1.5±0.2	1.5±0.1	
1.12×10^{16}	1.6±0.1	1.3±0.2	1.4±0.1	
1.31×10^{16}	1.6±0.1	1.3±0.1	1.7±0.1	
1.50×10^{16}	1.5±0.1	1.0±0.2	1.5±0.1	
2.44×10^{16}	1.5±0.1	1.7±0.1	1.4±0.1	
3.38×10^{16}	1.5±0.1	1.5±0.1	1.5±0.1	
4.31×10^{16}	1.5±0.1	1.7±0.1	1.7±0.1	
5.25×10^{16}	1.6±0.1	1.8±0.2	1.7±0.1	

Experiment Results: Defect density of sample M1 as deduced from NMR decay shape of the three isotopes following successive irradiations.

$1.49 \pm 0.2 \times 10^{14} cm^{-3}$ and $1.56 \pm 0.10 \times 10^{14} cm^{-3}$ as determined for the isotopes Ga^{69}, Ga^{71} and As^{75} respectively. As this result became evident the sample used by Cueman was also irradiated with a larger fluence per step and its defect density measured at room temperature. As can be seen from Table IV where the results for this sample are given, once again there is no significant change in the charged defect density of the sample. The defect density for this case is measured to be 1.86 ± 0.08, 1.9 ± 0.2 and $1.92 \pm 0.07 \times 10^{14} cm^{-3}$ for Ga^{69}, Ga^{71} and As^{75} respectively.

There also is no appreciable change in the carrier concentration. This was determined by the absence of a change in the shape of the free induction decay when the samples were taken from room temperature to liquid nitrogen temperature. As mentioned earlier, this implies there are not enough carriers present to affect the decay shape measurably.

This conclusion is in agreement with an independent measurement of the carrier concentration. A slice was taken off the sample. This slice was irradiated with the sample used in the NMR measurements at the Naval Research Lab. After each irradiation, its carrier concentration was measured there by N. Wilsey, using a method developed by Van der Pauw.[14,15] All the measured carrier concentrations were of order $10^{12} cm^{-3}$ or less. Since 10^{12} carriers (cm^{-3}) is the lower limit of the sensitivity of his equipment, carrier concentrations of this size would not affect the decay shape, as shown in Chapter III. Hence this measurement is consistent with the conclusions drawn from the lack of temperature variation of the decay shape.

TABLE IV

Total Fluence (cm^{-2})	Defect Density as Measured by Ga^{69}	Ga^{71}	As^{75} ($10^{14} cm^2$)
5.30×10^{16}	1.8±0.2	2.1±0.2	1.9±0.1
6.25×10^{16}	2.0±0.1	1.9±0.2	2.0±0.1
7.18×10^{16}	1.9±0.1	1.7±0.2	2.0±0.1
8.12×10^{16}	1.7±0.1	2.3±0.1	1.8±0.1
9.04×10^{16}	1.9±0.2	1.9±0.1	1.9±0.1
10.00×10^{16}	1.9±0.2	1.8±0.1	1.9±0.1
10.94×10^{16}	1.8±0.2	1.8±0.1	2.0±0.1
19.07×10^{16}	1.9±0.2	2.1±0.2	1.9±0.1

Experimental Results: Defect density of sample M8 as deduced from measurement on the three isotopes following successive irradiations.

Since we are unable to see a measurable increase in the number of charged defects or any appreciable change in the carrier concentration of the irradiated samples, the defects one would have expected to be created by the gamma irradiations are either uncharged at room temperature, or not present. Several experiments were designed to decide between these alternatives by changing the charge states of any unionized defects that were present. Attempts were made to ionize the defects thermally by raising the temperature of the crystal to 120°C (the highest temperature we dared to use because at 500°K the radiation damage is known to anneal out), and optically by shining light from a 1000 watt light source with a color temperature of ~4500°K on the sample. The resonance decay shape for the sample in both situations displayed no measurable change. Finally, the sample was annealed at 525°K in a dry N_2 atmosphere for fifteen minutes. Once again, the NMR decay shape was unaffected.

This collection of results points to the inescapable conclusion that no appreciable increase in the number of electrically active defects were introduced into our sample by the gamma irradiations. This is a rather unexpected result, and it makes one wonder what property of these samples causes them to be impervious to radiation damage. Some possibilities are discussed in Chapter VI.

B. The Carrier Concentration of Thermally Damaged Samples

One possible reason we are not able to measure an increase in the number of charged defects with irradiation is that the number of defects already in the sample was miscalibrated because of screening and it is actually much greater than the increase resulting from the gammas. The absolute defect density of the sample before irradiation was determined from an analysis by Cueman[9] of the resonances of some GaAs samples that were thermally damaged by Hester.[8] One of Cueman's assumptions that later became suspect, was that the carrier concentration was not large enough to affect the decay shape.

This assumption became of particular concern when the carrier concentrations of the samples were measured by D. C. Look at the Avionics Laboratory, Wright Patterson A.F.B. He measured the carrier concentrations for four samples, three of which were damaged at different temperatures. The fourth was damaged twice at two different temperatures. The carrier concentrations for the samples at room temperature were found to vary from sample to sample between $10^{14}cm^{-3}$ and $5 \times 10^{15}cm^{-3}$. As mentioned in Chapter IV, carrier concentrations of these magnitudes should have a measurable effect on the decay shape of the resonances of the sample.

In addition to measuring the carrier concentrations of the samples at room temperature, Look also measured the carrier concentrations as a function of temperature. He found that for three of the samples the carrier concentration dropped by several orders of magnitude, to 10^{9} to $10^{10}cm^{-3}$ at liquid nitrogen temperature, a level at which the carrier

should no longer have a measurable effect on the decay shape. In the case of the fourth sample, which was the sample damaged at the highest temperature, the carrier concentration decreased from about $5 \times 10^{15} cm^{-3}$ at room temperature to $2 \times 10^{14} cm^{-3}$ at liquid nitrogen temperature. Here although the carrier concentration is not negligible at liquid nitrogen temperature, a change of carrier concentration of this magnitude should result in an appreciable change in the decay shape of the resonance.

The free induction decays for the samples, at room temperatures were fitted in the manner described in Chapter IV, to find the carrier concentration as well as the defect density. The fitting parameter A_3 corresponding to the carrier concentration indicated that the carrier concentrations of the samples were much lower than those measured by Look. In addition, fits to the decay shape made by setting the carrier concentration equal to zero had χ^2 values two to seven times smaller than fits made assuming the value measured by Look. These fits had on the order of 700 degrees of freedom and χ^2's were about 2. Both of these results suggest the carrier concentration of the bulk sample is much less than the carrier concentrations measured by Look.

An examination of the decay shape of the resonance of the samples when they are at liquid nitrogen temperature tends to add validity to this suggestion. There is no evidence of the decay shape change one would expect from the temperature dependence Look finds for the carrier concentration. In fact, the free induction decays have no change in shape as the temperature of the sample is reduced to liquid nitrogen temperature. Therefore, once again, the carrier concentration does not appear to have an effect on the decay shape.

The charge carrier concentration measured by Look does not appear to be a property of the bulk sample, but is probably the carrier concentration at the surface. Thus, the approximation of Cueman that the bulk carrier concentration is too small to affect the decay shape appears to be correct.

C. Homogeneity of the Thermally Damaged Crystals

Another assumption made by Cueman about the thermally damaged samples was that the samples were homogeneous. This would be true if the samples were held at the elevated temperature long enough for them to come to an internal equilibrium. Whether or not the samples had been held at the elevated temperaturès long enough came under question in light of some new information.

In an experiment by Chiang and Pearson[16], a gallium arsenide single crystal was held at 800°C for 25.5 hours in an evacuated sealed quartz ampoule. By comparison, when Hester[8] thermally damages his samples, they were held at a maximum of 700°C for 24 hours in evacuated vycor vessels (these were the samples analyzed by Cueman). Following the thermal damage Chiang and Pearson measured the carrier concentration as a function of distance from the surface of the sample. They found the carrier concentration returned to its predamaged value after 4.3 microns. Therefore, they concluded that the vacancies are able to migrate only 4.5 microns from the surface, when the GaAs is held at 800°C for 25.5 hours.

In addition, Van Vechten estimated that the penetration depth of a neutral vacancy is 31 microns for GaAs held at 700°C for 24 hours[17]. If the mechanism for the thermal damage of Hester's samples is the migration of arsenic vacancies from the surface through the crystal, then from the two results quoted above, one would expect all the damage to reside very close to the surface of the sample, since the dimensions of the samples are approximately 0.6 cm by 0.6 cm by 1.1 cm.

To test the homogeneity of the samples, they were sliced into three parts of equal size, with cuts along the long axis and parallel to one of the faces of the sample. Free induction decays were taken from the center piece and one of the side pieces. Only the resonances from the As^{75} and Ga^{69} isotopes were examined since from the gamma experiment they appeared to be the most sensitive. The defect densities of the slices found by fitting the free induction decays, assuming the carrier concentration to be zero, are given in Table V.

From the defect densities found for each slice it would appear the samples were close to being homogeneous, if not completely homogeneous. Knowing the samples are almost homogeneous, the time the samples were held at the elevated temperature and the size of the sample makes it possible to set a lower limit on the diffusion constant, as is done in Chapter VI.

An important aspect of the result in Table V is that the defect densities deduced from the Ga^{69} decay shape are significantly larger than the defect densities deduced from the As^{75} decay shape. Contrast this with the results of the gamma experiment (Table III) where the defect

TABLE V

DEFECT DENSITIES OF DIFFERENT SECTIONS

OF THE THERMALLY DAMAGED SAMPLES

Sample	Quench Temp (^{o}C)	Isotope	Defect Density (10^{14}cm^{-3})		
			Whole sample	Midsection	Side Section
M2	550	Ga^{69}	3.1 ± 0.1	5.0 ± 0.1	4.5 ± 0.1
M2	550	As^{75}	2.8 ± 0.1	2.8 ± 0.1	3.7 ± 0.1
M7	600	Ga^{69}	5.6 ± 0.1	5.9 ± 0.1	6.6 ± 0.2
M7	600	As^{75}	4.3 ± 0.2	4.7 ± 0.1	4.1 ± 0.2
M5	700	Ga^{69}	4.4 ± 0.1	2.8 ± 0.1	4.5 ± 0.1
M5	700	As^{75}	3.5 ± 0.1	4.1 ± 0.1	3.7 ± 0.1

densities deduced from the measurements on all three isotopes are the same within experimental error. This is evidence for failure of Eq. (28) at these higher defect densities and indicates, at least for As^{75}, that the value of the defect density found by applying the theory is incorrect. Indeed, the measured defect densities for all three samples exceed the validity condition for As^{75} (see Eq. (28)). Even though the absolute defect densities determined from the decay shapes may not be accurate because the measurement is saturating, the ratio of the defect densities of the midsection to side section provide an upper bound to the true ratio that is useful in estimating the diffusion constant. This is done in Chapter VI.

VI. DISCUSSION

A. Radiation Damage of Gallium Arsenide

The typical radiation damage experiment of GaAs is to irradiate it with electrons or gamma rays and measure the change in charge carrier concentration. The irradiations are found always to reduce the carrier concentration for n- and p-type samples. The change in carrier concentration divided by the fluence of the irradiating particle is called the carrier depletion rate. Brailoskii and Knonzenko[18] measure the carrier depletion rate to be $1.4 \times 10^{-2} cm^{-1}$ for a single crystal of n-type GaAs irradiated by gamma rays at room temperature.

Electron irradiations of GaAs at room temperature show the depletion rate of n- and p-type materials are the same. One would then expect that irradiations at room temperature to produce equal numbers of deep acceptors and deep donors. In n-type material, the acceptors serve as electron traps, while the donors created are too deep to affect the carrier concentration. The reverse is true in p-type material.

The GaAs used in this experiment had a carrier concentration of $2 \times 10^{11} cm^{-3}$ before irradiation. If a one-to-one correspondence between the creation of acceptors and the removal of carriers is assumed, the depletion rate determined by Braileskii and Konozenko gives the density of donors and acceptors created for the smallest dose of irradiation of the sample as $1.5 \times 10^{13} cm^{-3}$. This figure is much greater than

the carrier concentration of the sample before the irradiation. The acceptors and donors should then compensate each other and both become charged. Assuming this happens, after the final irradiation of the sample which received the greatest total fluence of gamma rays, the net increase in the charged defect density should be $4.8 \times 10^{15} cm^{-3}$. This is approximately ten times the defect density prior to irradiation and is much greater still than the estimated sensitivity ($5 \times 10^{13} cm^{-3}$) of the measurement technique. It was somewhat disconcerting when there was little or no change in the measured defect density upon irradiation.

With this in mind, it became necessary to consider these results in light of experiments done by others to see if some model could be proposed that explains all these results. One important observation is that the crystal used in our experiment is not typical of crystals normally used in radiation damage experiments. The lowest carrier concentrations for crystals normally used in these experiments are on the order of $10^{16} cm^{-3}$, four orders of magnitude greater than our sample. Equally important is that the charged defect density for our sample is lower by two orders of magnitude, making the average distance between charged defects a factor of 4 times greater for our crystal.

To emphasize my previous remarks, the carrier concentration, as determined by many experiments always decreases[3,18] during irradiation. Comparisons between the depletion rate in p-type and n-type GaAs irradiated at room temperature indicate that the depletion rate is independent of the type of the majority carrier.[19,20,21] The depletion rate has been measured for crystals starting with carrier concentrations

varying from 10^{16} to $10^{18}cm^{-3}$, and no dependence on the initial carrier concentration was found.

For GaAs irradiated at liquid nitrogen temperature, the carrier concentration returns to its pre-irradiated value in three annealling stages.[22] The kinetics of the first two were studied by Thommen.[22] He showed both stages, which appear at 235°K and 280°K, are the result of first order processes. The first order process indicates that one of the defects is mobile at these temperatures and moves until it finds another defect, or wanders out of the crystal. Therefore, from these annealling stages it would appear at least one of the defects created by the irradiation (possible two) is mobile at room temperature. This annealling stage returns the carrier concentration to within 10 to 20% of its original value.

The third annealling stage occurs above room temperature at 500°K. It returns the carrier concentration to its original value. The kinetics of this stage have been studied by Aukerman and Graft.[3] They found this stage to be the result of a combination of two first order processes. The first process is independent of the initial carrier concentration of the sample irradiated. The annealling rate of the second process is dependent on the pre-irradiated carrier concentration to the 2/3 power. Lang[1] interprets this second process as being the migration of the defects to donors in the crystal.

Jeong et. al.[5] have been able to identify at least one of the defects that is mobile in the 500°K annealling stage. Using photoluminescence on a Si-doped GaAs crystal, they focus on a particular

spectral peak. By a series of experiments, they identify this peak as arising from a complex between an arsenic vacancy and a silicon atom on an arsenic site. After identifying the source of the peak, they irradiate the sample with electrons at 77°K. After the irradiation, the sample is slowly brought up from 77°K, in order to observe each of the annealling stages. The intensity of the photoluminescence spectrum is reduced considerably from its pre-irradiated level until the 500°K annealling stage is reached. Then the intensity of the entire spectrum returns to its original value. The particular peak that they had identified was enhanced by the process of irradiation and annealling. They therefore conclude that the 500°K annealling stage is a result of the mobility of the arsenic vacancy.

Such annealling experiments, while yielding some information about the nature of the defects, do not produce a complete picture of all the defects. The only way to characterize the individual stable defects created by irradiation is through their electronic energy levels. For electron and hole traps, Lang and Kimerling[4] have done this by using a method they named deep-level transient spectroscopy (DLTS). They find irradiation at room temperature forms five different types of electron traps. Each of these five traps has its own introduction rate. Since the four simple defects (Ga interstitial and vacancy, and As interstitial and vacancy) always come in pairs, there are only two possible different introduction rates for the elemental defects. The existence of five different introduction rates thus provides clear evidence that at least some of the traps are complexes.

Our experiment, which measures the total number of separated charged defects in the bulk, indicates that the number of charged defects in the sample does not change with irradiation, at least for very pure material. It also demonstrates that the carrier concentration of these samples does not change appreciably. No model has been suggested that explains our results and at the same time is consistent with the experimental results of others. An acceptable model must be in agreement with the following observations. (1) For a crystal with a carrier concentration on the order of $10^{16}cm^{-3}$ or greater, irradiation reduces the carrier concentration present initially, regardless of the type of the majority carrier. If there is a one-to-one correspondence between the removal of a majority carrier and the formation of a defect, then the number of donors created by a given fluence of irradiation in a p-type sample of GaAs must be equal to the number of acceptors produced by a similar fluence in n-type GaAs. (2) When the initial carrier concentration is on the order of $10^{11}cm^{-3}$ or greater. There is also no type change when the starting material is n-type.

One is tempted to model explanations of our results that rely on the assumed properties of a number of complexes. However, the experimental results quoted above place constraints on the nature of these complexes. First, any complexing must not change the magnitude of the charge on an impurity that becomes a member of a complex unless it is accompanied by a change of the charge on an impurity elsewhere in the crystal. Any change of the charge on an impurity changes the electric field around the defect and, therefore, would change the quadrupole

splitting of the nuclei around the defect. This would result in a change of the shape of the free induction decay. Since we see no change in the shape of the free induction decay for our sample, any change of the magnitude of the charge on an impurity, as the result of complexing, must be accompanied by a change of the magnitude of the charge on another impurity elsewhere in the sample to keep the net quadrupole broadening the same. This is not likely, especially since partial effective charges may be involved, hence the model would have to suppose that the charge states of defects are unchanged when they form complexes.

Complexes that result in defect type changes (e.g., donors that after complexing become acceptors) are a special case of the above argument. If a donor converts to an acceptor, there must be a complementary change of an acceptor to a donor somewhere else. Otherwise, there would have to be a change in the carrier concentration, contrary to our observations. Once again, while some workers have suggested such type changes,[23] in our samples the data indicates that such effects are unlikely.

Another problem arises from explaining our data by saying that the only stable defects are complexes. This is the explanation of the 500°K annealling stage. This stage is well documented, for many different samples with different impurities, growth techniques and type. The fact that all these crystals revert to their pre-irradiated characteristics at the 500°K anneal means that the complexes formed must revert to their pre-irradiated form after the 500°K

anneal. This would indicate one of two things, both of which seem unlikely. Either all the different crystals have some common impurity or defect which complexes with the elemental defect formed by the radiation, or the bonding energy of the elemental defect and the particular impurity with which they complex is a function only of some characteristic property of GaAs. One of these features is needed to explain why the complexes always disassociate at 500°K. These features are further complicated by the experimental results of Jeong et. al., i.e., the Si-As vacancy complexes did not form until after this same 500°K anneal. This poses the question of why these form at the same temperature while others are disassociating, and yet do not form at lower temperatures.

The difficulties that arise from trying to explain our results by complexes, lead one to believe that the proper explanation is that the defects created by irradiation have annealled out. Consider the following model. Vacancies and interstitial atoms are mobile at room temperature until they have formed a complex with another defect, which they do readily. The radiation produces Frenkel pairs that either form complexes, or they recombine with a relative probability that depends on the defect concentration of the starting material. If the starting material has a high defect density, then the Frenkel pairs complex before they can recombine. If the material is sufficiently pure the reverse is true, therefore the result of the irradiation is no permanent damage. If this model is correct, then the self diffusion should be faster in sufficiently pure samples than in samples with higher defect densities. We have alluded to fast diffusion in the thermal damage studies in Chapter V, and will

elaborate on it in the next section. Then the reason we saw no radiation damage, in contrast to other investigators, is the greater purity of our starting material.

While the greater purity of our sample obviously produces the desired qualitative trend to explain our data in terms of the proposed model, there remains troublesome quantitative questions. The first is that others find no change in the depletion rate of carriers due to irradiation in GaAs samples, with carrier concentrations varying from 10^{16} to $10^{18} cm^{-3}$ and impurity concentrations varying from about $1.5 \times 10^{16} cm^{-3}$ to $10^{18} cm^{-3}$. For such a large decrease in the damage rate to occur when the defect density drops from approximately $1.5 \times 10^{16} cm^{-3}$ to $5 \times 10^{14} cm^{-3}$ requires some additional explanation.

The second question arises from a quantitative discussion of the damage that should have been created in the sample recieving the highest gamma ray fluence. If the damage is created uniformly in the crystal, then some of the displaced atoms will be located near an existing defect. If our model is correct, these defects will not anneal, and permanent radiation damage results.

We expected to create a defect density of $4.8 \times 10^{15} cm^{-3}$ in the crystal recieving the largest gamma ray fluence. About 3% of these (or $1.5 \times 10^{14} cm^{-3}$) will be as close to a native defect as the average damage center would be in a crystal that started with a defect density of $1.5 \times 10^{16} cm^{-3}$. Since we assume an initial defect density of $1.5 \times 10^{16} cm^{-3}$ will prevent annealling then these 3% should not

anneal. However, an increase of $1.5 \times 10^{14} cm^{-3}$ is several times larger than our sensitivity, and should have been detected. Some addition to our model must be made to account for the absence of this residual damage.

One possible mechanism suggested by these results is that rather than the defects created by radiation being trapped on individual impurities, they are trapped by a collective effort of the impurities already present in the crystal. For this collective effort to be effective, the average separation between impurities must be less than some critical value. For our case, the average separation between impurities is greater than this critical value, and the collective effort is not an effective deterent to annealling. Therefore, the defects anneal out before they are seen. Unfortunately, at this time we have no support for this idea, other than it could explain the observations.

Another explanation to be considered is that the vacancies created by irradiation of the sample can complex only with a particular type of impurity in the crystal. In addition these impurities can accommodate only one vacancy. Then for our case where the purity of the sample is much greater than those normally used in radiation experiments, these impurities were already complexed with the vacancies in the as grown crystal, leaving few free to stablize the defects created by the irradiation. As a result, we saw no increase in the number of defects with irradiation.

The difficulties that arise from trying to explain the lack of charged defects introduced by irradiation lead one to believe that the proper explanation is that the defects created by irradiation have annealled.

It is impossible with the information at hand, to be sure what is happening when the crystal is irradiated. Several experiments could be performed that might help untangle this mystery. First, it would be of interest to perform the irradiations and the initial NMR measurements in liquid nitrogen. This would make it possible to examine the damage below the low temperature annealling stages. Then, it would be interesting, if any defects are introduced, to examine how they change as the sample is brought through the first two annealling stages.

A second type of experiment that should yield some interesting information would start with a very pure, uncompensated crystal with carrier concentration of about $10^{15}cm^{-3}$. Then, monitoring the change in carrier concentration and NMR decay shape as a function of fluence would give a clearer indication of whether or not the crystal is changing with irradiation. This also yields data on the relationship between the change in carrier concentration and charged defect density.

B. Diffusion

Comparing the relative defect density of the middle slabs of the thermally damaged crystals to the side slabs, it becomes apparent that diffusion rates recorded in the literature are much too small to account for our observations. It is of interest to estimate a diffusion rate that would explain this result.

If the diffusion coefficient D is a constant, the equation for the diffusion of a substance through the sample is given by the expression[24]

$$\frac{1}{D}\frac{\partial C}{\partial t} = \nabla^2 C , \tag{30}$$

where C is the concentration of the diffusing substance.

For the case of a rectangular parallelpiped, this equation often can be solved by the method of separation of variables, i.e., by assuming a solution of the form

$$C(x,y,z,t) = X(x)\,Y(y)\,Z(z)\,T(t). \tag{31}$$

Substitution of Eq. (31) into Eq. (30) allows separation into three independent spatial equations and a fourth time dependent equation related to the other three by a constant. The four equations are

$$\frac{\partial^2 X}{\partial x^2} + a^2 X = 0, \tag{32a}$$

$$\frac{\partial^2 Y}{\partial y^2} + b^2 Y = 0, \tag{32b}$$

$$\frac{\partial^2 Z}{\partial z^2} + c^2 Z = 0, \tag{32c}$$

and

$$\frac{\partial T}{\partial t} + (a^2 + b^2 + c^2)\,T(t) = 0 . \tag{32d}$$

For a sample extending from $-\ell_x$ to ℓ_x in the x direction with walls at these points held at concentrations C_1, and the sample being initially homogeneous with concentration C_o, the solution for

the x direction is given by the expression

$$C(x,t) = C_0 + (C_1 - C_0)\, F(x,t), \tag{33}$$

where

$$F(x,t) = 1 + \frac{4}{\pi} \sum_{n=0}^{\infty} \frac{(-1)^n}{2n+1} \exp\left\{-D(2n+1)^2 \frac{\pi^2 t}{4\ell_x^2}\right\} \cos\frac{2n+1}{2\ell_x}\pi x \tag{34}$$

Our sample approximately from $-\ell_x$ to ℓ_x in the x and y directions and from $-\ell_z$ to ℓ_z in the z direction. The six sides of the sample are held at a constant concentration of vacancies (C_1) determined by the vapor pressure of As and the solubility of the arsenic vacancies in the GaAs crystal. The crystal is initially homogeneous, with a concentration of defects C_0. Since

$$e^{a+b} = e^a e^b \tag{35}$$

the concentration of defects as a function of time and position in the sample is given by

$$C(x,y,z,t) = C_0 + (C_1 - C_0)\left\{F(x,t)\, F(y,t)\, F(z,t)\right\}. \tag{36}$$

For long times, when the sample is close to equilibrium, only terms of order $\exp\left\{-D\pi^2 t/4\ell_x^2\right\}$ are going to make significant contributions to the summation. Saving only such terms, we may rewrite Eq. (36) as

$$C(x,y,z,t) = C_0 + (C_1 - C_0)\left\{1 - \frac{4}{\pi}\left(\exp\left(-\frac{D\pi^2 t}{4\ell_x^2}\right)\left(\cos\frac{\pi x}{2\ell_x} + \cos\frac{\pi y}{2\ell_y}\right)\right.\right. \tag{37}$$
$$\left.\left. + \exp\left(-\frac{D\pi^2 t}{4\ell_z^2}\right)\cos\frac{\pi z}{2\ell_z}\right)\right\}.$$

The average concentration in any section of the sample is the total number of defects in that region divided by the volume of the region. Conversely, the total number of defects is equal to the integral of the concentration over the volume. For the middle section of our sample, with cuts parallel to the x faces of the sample, the total number of vacancies in the middle section of the sample (N_{ms}) is then

$$N_{ms} = \int_{-\ell_x/2}^{\ell_x/2} dx \int_{-\ell_y}^{\ell_y} dy \int_{-\ell_z}^{\ell_z} dz\, C(x,y,z,t) = \frac{1}{3} V C_0 + \frac{1}{3} V (C_1 - C_0) \left\{ 1 - \frac{20}{\pi^2} e^{-D\pi^2 t / 2\ell_x^2} - \frac{8}{\pi^2} e^{-D\pi^2 t / 4\ell_z^2} \right\}, \quad (38)$$

where V is the volume of the sample. The total number of defects in one of the side sections is

$$N_{ss} = \int_{\ell_x/3}^{\ell_x} dx \int_{-\ell_x}^{\ell_x} dy \int_{-\ell_z}^{\ell_z} dz\, C(x,y,z,t) = \frac{1}{3} V C_0 + \frac{1}{3} V (C_1 - C_0) \left\{ 1 - \frac{14}{\pi^2} e^{-\frac{D\pi^2 t}{4\ell_x^2}} - \frac{8}{\pi^2} e^{-\frac{D\pi^2 t}{4\ell_z^2}} \right\}. \quad (39)$$

The ratio R of the change in the average concentrations of the two sections, since the volumes are equal, is given

$$R = \frac{N_{ms} - \frac{1}{3} V C_0}{N_{ss} - \frac{1}{3} V C_0} = \frac{1 - \left(\frac{20}{\pi^2} e^{-D\pi^2 t / 4\ell_x^2} + \frac{8}{\pi^2} e^{-D\pi^2 t / 4\ell_z^2} \right)}{1 - \left(\frac{14}{\pi^2} e^{-D\pi^2 t / 4\ell_x^2} + \frac{8}{\pi^2} e^{-D\pi^2 t / 4\ell_z^2} \right)} \quad (40)$$

Solving this equation for D leads to the transcendental equation

$$(R-1) + \frac{2 e^{-D\pi^2 t / 4\ell_x^2}}{\pi^2} (10 - 7R) + \frac{8}{\pi^2} e^{-D\pi^2 t / 4\ell_z^2} (1 - R) = 0. \quad (41)$$

Eq. (41) is solved numerically only for those cases where $R \lesssim 1$. These results give a lower limit on the diffusion constant for the samples, at the thermal damage temperatures. The results are shown in Table VI.

While the results in Table VI provide a lower limit to the diffusion constant at the higher temperatures, the absence of any motional narrowing of the NMR line offers an upper limit to D. Motional narrowing becomes a factor when the correlation time for diffusion (τ_c) is of the order of the spin-spin relaxation time (T_2) for the nuclei. The correlation time is related to D by the equation

$$\tau_c = \frac{1}{2}\frac{d^2}{D} \tag{42}$$

where d is the distance between like neighbors. The thermal dependence of D is given by the expression

$$D = D_o \exp(-Q/kT) \tag{43}$$

where Q is the activation energy and D_o is the limiting diffusion constant at infinite temperature. Values for Q and D_o must fall in a region that is limited by our two estimates of D.

The first condition no motional narrowing of the resonance line means that the correlation time is greater than T_2. The longest T_2 for any of the free induction decays of GaAs is about 200 microseconds. The highest temperature at which a sample has been held while looking at the free induction decay is about 120°C (400°K). No motional narrowing was seen for that temperature, therefore, it is used to set the upper limit on the diffusion constant. By using

TABLE VI

Ratio of change[X] in defect density of Midsection to change in defect density of Side section (R)	Temperature (^{o}C)	D(cm^2/sec)
0.5 ± 0.04	550°C	(2.8 ± 0.6) x 10^{-6}
0.87 ± 0.09	600°C	(3.9 ± 0.6) x 10^{-6}
0.77 ± 0.07	600°C	(3.3 ± 0.6) x 10^{-6}
0.42 ± 0.01	700°C	(2.7 ± 0.6) x 10^{-6}

[X] initial defect density of all samples assumed to be 1.9 x $10^{14}cm^{-3}$

Diffusion constants calculated from the ratio of the defect density of the middle slice to the side slice of the thermally damaged samples

Eqs. (42) and (43), we find D_o and Q must fall in a region where by the expression

$$D_o < \left(\tfrac{1}{2}\frac{d}{200\mu sec}\right) \exp\left(Q/k(400^\circ K)\right). \qquad (44)$$

The second condition the thermally damaged samples being nearly homogeneous leads to the diffusion constant being greater than or equal to those values for diffusion constants found in Table VI. There the lower limit on the diffusion constant at 550°C is found to be $2.8 \times 10^{-6} cm^2/sec$. This confines D_o and Q to a region defined by

$$D_o > (2.8 \times 10^{-6} cm^2/sec) \exp\left(Q/k(820^\circ K)\right) \qquad (45)$$

The region in which both conditions are satisfied is shown graphically in Fig. 10.

The lower portion of this region has D_o's which are comparable to that quoted for GaAs in the literature of 0.7 cm^2/sec.[27] However, the activation energy for such D's is a factor of 3 below the reported value of 3.2 eV.[27] The higher purity of our samples can also explain the rapid diffusion rates we find compared to those measured in less pure samples. If the vacancies that contribute to the self diffusion are trapped out in complexes in the less pure samples, then the rapid diffusion in the pure samples would be understandable. Once again additional measurements are needed to confirm this hypothesis.

A better measurement of the diffusion constant can be obtained at lower temperatures by measuring $T_{1\rho}$, employing the method pioneered by Slichter and Ailion.[28] $T_{1\rho}$ is the lifetime of the local order of the

Figure 10. Region of acceptable Q's and D_o's

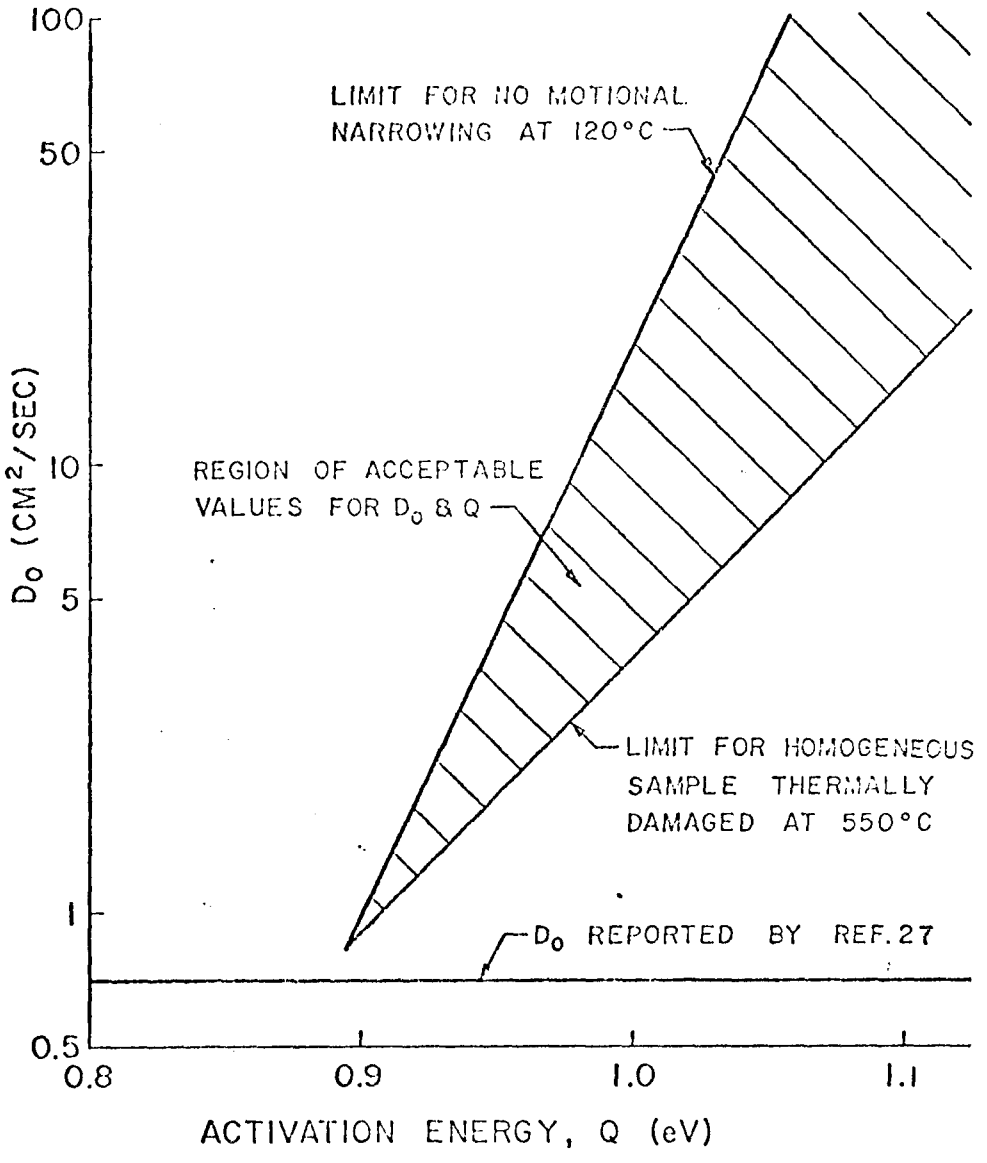
100
50
10
5
1
0.5
D_o (CM^2/SEC)
LIMIT FOR NO MOTIONAL NARROWING AT 120°C
REGION OF ACCEPTABLE VALUES FOR D_o & Q
LIMIT FOR HOMOGENEOUS SAMPLE THERMALLY DAMAGED AT 550°C
D_o REPORTED BY REF. 27
0.8
0.9
1.0
1.1
ACTIVATION ENERGY, Q (eV)

spin system, which is very sensitive to the motion of the nuclei through the lattice. By measuring $T_{1\rho}$, it is possible to measure correlation times that are less than the usual spin-lattice relaxation time (T_1). For the arsenic resonance T_1 is approximately 0.33 seconds at room temperature. Therefore, using this method, it should be possible to measure the diffusion constant at room temperature if it is greater than $2 \times 10^{-15} cm^2/sec$. If the diffusion constant is greater than $2 \times 10^{-15} cm^2/sec$, however, it would be too large to be accounted for by the D_o's and Q's found in the region defined by Fig. 10. Therefore, at room temperature we would not expect to encounter such a rate. However, at higher temperature, say 120°C, one should be able to measure the diffusion constant if it is as large as expected from the thermal damage studies. For this temperature, T_1 is 0.13 sec.[29] Therefore the diffusion constant should be measurable if Q is less than 1.3 eV and D_o is less than 310 cm^2/sec.

The most important results of this experiment are the conclusion that in high purity GaAs there is no stable, permanent radiation damage, and the diffusion constant is greater than in samples which are less pure. The reason for both effects appears to be that the impurities present in the crystal impede the motion of the vacancies in the lattice. A controlled measurement of the diffusion constant in different samples of high purity is needed to understand completely the mechanisms involved.

VII. REFERENCES

1. D. V. Lang, "International Conference on Radiation Effects in Semiconductors," Dubrovnik, Yugoslavia (1976), (Inst. Phys. London (1977)), p. 70.
2. L. W. Aukerman, Semiconductors and Semimetals, v. 4, Ed. by R. K. Willardson and A. C. Beer, Academic Press, New York, 1968, p. 343.
3. L. W. Aukerman and R. D. Graft, Phys. Rev. 127, 1576 (1962).
4. D. V. Lang and L. C. Kimerling, "Lattice Defects in Semiconductors" (1974) (Inst. Phys. Conf. Ser. 23) (1975)) p. 581.
5. M. V. Jeong, J. Shirafugi and Y. Inuishi, Jap. J. Appl. Phys. 12, 109 (1973).
6. P. A. Fedders, Phys. Rev. B11, 1020, (1974).
7. M. K. Cueman, R. K. Hester, A. Sher, J. F. Soest and I. J. Lowe, Phys. Rev. B12, 3610 (1975).
8. R. K. Hester, unpublished Ph.D. dissertation, College of William and Mary, 1975.
9. M. K. Cueman, unpublished Ph.D. dissertation, College of William and Mary, 1975.
10. A. N. Garroway and D. Ware, Rev. Sci. Instrum. 46, 1342 (1975).
11. A. M. Stoneham, Rev. Mod. Phys. 41, 82 (1969).
12. M. H. Cohen and R. Reif, Solid State Phys. 5, 322 (1957).
13. D. Gill and N. Bloemberger, Phys. Rev. 129, 2398 (1963).

14. L. J. Van der Pauw, Philips Res. Repts. 13, 1 (1958).

15. L. J. Van der Pauw, Philips Technical Rev. 20, 220 (1959).

16. S. Y. Chiang and G. L. Pearson, J. Appl. Phys. 46, 2986 (1975).

17. J. A. Van Vechten, private communication.

18. E. Y. Brailouskii and L. D. Konozenko. Sov. Phys. Semicon. 5, 563 (1971).

19. N. A. Vitovskii, T. V. Mashovets, S. M. Ryvkin and R. Yukhansevarou, Sov. Phys. - Solid St. 5, 2575 (1964).

20. A. H. Kalma and R. A. Berger, IEEE Trans. Nucl. Sci. NS-19, 209 (1972).

21. P. L. Pegler, T. A. Grimshaw and P. C. Banbury, Radiat. Effects 15, 183 (1972).

22. K. Thommen, Radiat. Effects 2, 201 (1970.

23. D. T. J. Hurle, "International Symposium on Gallium Arsenide and Related Compounds," 6th, Edinburgh (1976) (Inst. Phys. London (1977)), p. 113.

24. J. Crank, The Mathematics of Diffusion, Oxford U. P. London, p. 24.

25. Ibid., p. 47.

26. Abragam, The Principles of Nuclear Magnetism, Oxford U. P. London, 1964, p. 441.

27. H. C. Casey, Jr., and G. L. Pearson, Point Defects in Solids, v. 2, Ed. by J. H. Crawford, Jr., and L. M. Sliflein, Plenum Press, New York, 1975, p. 163.

28. C. P. Slichter and D. C. Ailion, Phys. Rev. A135, 1099 (1964).

29. W. G. Clark, Phys. Rev. 164, 288 (1967).